Nature. Author manuscript; available in PMC 2015 June 04.

Published in final edited form as:
Nature. 2014 December 4; 516(7529): 94–98. doi:10.1038/nature13960.

An enteric virus can replace the beneficial function of commensal bacteria

Elisabeth Kernbauer[1,2], **Yi Ding**[3], and **Ken Cadwell**[1,2]

[1]Kimmel Center for Biology and Medicine at the Skirball Institute, New York University School of Medicine, New York, NY 10016, USA

[2]Department of Microbiology, New York University School of Medicine, New York, NY 10016, USA

[3]New York Presbyterian Hospital, New York, NY 10065, USA

Abstract

Intestinal microbial communities have profound effects on host physiology[1]. Whereas the symbiotic contribution of commensal bacteria is well established, the role of eukaryotic viruses that are present in the gastrointestinal tract under homeostatic conditions is undefined[2,3]. Here, we demonstrate that a common enteric RNA virus can replace the beneficial function of commensal bacteria in the intestine. Murine norovirus (MNV) infection of germfree or antibiotics-treated mice restored intestinal morphology and lymphocyte function without inducing overt inflammation and disease. The presence of MNV also suppressed an expansion of group 2 innate lymphoid cells (ILCs) observed in the absence of bacteria, and induced transcriptional changes in the intestine associated with immune development and type I interferon (IFN) signaling. Consistent with this observation, the IFNα receptor was essential for the ability of MNV to compensate for bacterial depletion. Importantly, MNV infection offset the deleterious effect of antibiotics-treatment in models of intestinal injury and pathogenic bacterial infection. These data indicate that eukaryotic viruses have the capacity to support intestinal homeostasis and shape mucosal immunity akin to commensal bacteria.

Despite significant limitations in the ability to detect and annotate eukaryotic viruses present in the gastrointestinal tract, recent deep sequencing efforts reveal the existence of a complex enteric virome[3, 4]. Members of this viral component of the intestinal microbiota could include pathogens such as noroviruses that continue to persist after disease is resolved[5], *Anelloviridae* and *Circoviridae* family members that are ubiquitously detected in healthy individuals[6-8], and uncharacterized viruses that display little sequence identity with known

*To whom correspondence should be addressed: Ken Cadwell, Ph.D. New York University School of Medicine, Skirball Institute Lab 2-10, 540 First Avenue, New York, NY 10016. Telephone: (212) 263-8891. Fax: (212) 263-5711. ken.cadwell@med.nyu.edu.
Author contributions: E.K. performed all the experiments, Y.D. analyzed and scored histological sections, K.C. and E.K. designed the study and wrote the manuscript.

Author information (data storage): GEO accession number GSE60163 for RNAseq data. NCBI accession number KM463105 for MNV.SKI capsid sequence.

Authors declare no conflict of interest.

Europe PMC Funders Author Manuscripts

viruses[9-11]. Also, examination of the enteric virome of rhesus monkeys infected with simian immunodeficiency virus (SIV) suggest that many viruses are present at low levels and kept in check by the immune system[12]. Evidence that such viruses in the intestine can contribute to physiology beyond acute diarrheal disease is provided by studies examining MNV, a positive-strand RNA virus of the Caliciviridae family that is endemic in mouse facilities[13]. MNV displays tropism for myeloid cells and can establish persistent infection without causing obvious disease in immunocompetent mice[13, 14]. We recently demonstrated that persistent infection by the MNV strain CR6 (MNV.CR6) induces intestinal pathologies in mice deficient in the inflammatory bowel disease (IBD) gene *Atg16L1*[15]. This observation that MNV induces inflammatory pathologies in a genetically susceptible host resembles similar observations made with commensal bacteria. However, the bacterial component of the microbiota also provides significant benefit to the host by generating metabolites, promoting the development of the mucosal immune system, and preventing colonization by pathogenic microorganisms[1]. It is unknown whether eukaryotic viruses in the intestine interact with the host in an analogous symbiotic manner.

Much of our knowledge on the role of commensal bacteria in mucosal immunity comes from characterization of germfree (GF) mice, which display aberrant intestinal morphology and deficiencies in the lymphocyte compartment due to the absence of bacteria[16]. Thus, we utilized GF mice as a reductionist model to determine if MNV infection can provide developmental cues that have been mainly attributed to bacteria. GF mice were mono-associated with MNV.CR6 (GF+MNV) in a gnotobiotic isolator by infecting breeding pairs with 3×10^6 plaque forming units (PFU) and allowing the virus to be naturally propagated to offspring in subsequent generations, analogous to newborns that inherit commensal bacteria from parents (Extended data Fig. 1a). Despite persistent presence of the virus, there were no signs of overt inflammation in the intestine (Extended data Fig. 1b-d).

While GF mice had thin villi containing few $CD3^+$ T cells and narrow crypts, the general appearance of the small intestine (SI) in GF+MNV mice resembled that of conventional mice (Fig. 1a-f). The presence of virus in GF mice also partially restored the number of granules and lysozyme expression in Paneth cells (Extended data Fig. 2a-d). These changes in appearance due to MNV.CR6 were associated with a significant increase in the overall cellularity of the lamina propria (LP) and mesenteric lymph nodes (MLNs) (Fig. 1g, h). Consistent with the ability of certain bacterial species to promote lymphocyte differentiation[1], GF mice had reductions in the numbers of $CD4^+$ T cells in the LP and MLNs, $CD8^+$ T cells in MLNs, interferon (IFN)-γ expression by these cells, and mucosal and serum antibody production (Extended data Fig. 2e-p). In contrast, GF+MNV mice displayed increases in these factors, in some cases to an extent similar to or in excess of conventional mice (Extended data Fig. 2e-p). These effects of the virus were not dependent on neonatal infection since reversal of abnormalities was observed when adult GF mice were infected with MNV.CR6 for 10 days (Extended data Fig. 3). Also, the effects of MNV.CR6 cannot be explained by uncontrolled viral replication because GF mice harbor less virus compared to conventional mice upon infection (Extended data Fig. 1b), as seen with other intestinal viruses[17, 18]. Importantly, these changes in response to MNV.CR6 are specific to conditions in which bacteria are absent. MNV.CR6 had little or no effect on the appearance

of the intestine and lymphocytes in conventional mice (Extended data Fig. 4). Therefore, there is significant overlap in responses to MNV and commensal bacteria.

The host response evoked by MNV could depend on anatomical location or the strain examined. Abnormalities in the morphology of the colon of GF mice were not as apparent as in the small intestine, but we detected a significant increase in NKT cells[19]. While MNV mono-association had little effect on tissue morphology or the number of NKT cells, the presence of the virus increased the frequencies of both $CD4^+$ and $CD8^+$ T cells in the colon (Extended data figure 5). To determine whether the effect of MNV is specific to the CR6 strain, we infected GF mice with MNV.CW3, a strain that is considered more relevant to human noroviruses because it displays increased virulence compared to MNV.CR6 and establishes an acute infection[20]. Unlike conventional mice that clear the virus between days 5-7 post-infection[20], we found that a low amount of MNV.CW3 can be detected in stool of GF mice on day 10 post-infection (Extended data Fig. 1b), and was able to induce similar effects on intestinal morphology and the lymphocyte compartment as MNV.CR6 (Extended data Fig. 6b-h). Next, we isolated virus directly from a naturally infected mouse housed in the vivarium (MNV.SKI, described in Extended methods section). Alignment of the capsid sequence determined that MNV.SKI is a previously uncharacterized strain (Extended data Fig. 6a). MNV.SKI was also able to reverse abnormalities in GF mice (Extended data Fig. 6b-h). Although all three MNV strains induce qualitatively similar alterations to intestinal morphology and lymphocytes, the effects are quantitatively distinct, especially when comparing T cell subsets. Nevertheless, the general ability of MNV to evoke a response in GF mice appears to be strain-independent.

Innate lymphoid cells (ILCs) are emerging as important participants in mucosal immunity, but the role of the microbiota in maintaining this compartment is less understood. Unlike the skin and lungs, the intestine has been shown to contain reduced numbers of $Gata3^+$ ILC2s relative to $Rorgt^+$ ILC3s[21]. We found that GF mice had an increase in the proportion of ILC2s in the SI compared to conventional mice (Fig. 1i-m). This expansion of ILC2s due to the absence of bacteria was reversed in GF+MNV mice (Fig. 1i-m). Consistent with this finding, MNV.CR6 infection increased the proportion of ILCs expressing IL-22 relative to IL-13, effector cytokines expressed by ILC3s and ILC2s respectively (Fig. 1i, m). The proportion of the $T\text{-}bet^+$ ILC1 subset was similar across conditions (Extended data Fig 2q). Thus, we find that commensal bacteria prevent expansion of intestinal ILC2s, and MNV.CR6 infection mimics this function of commensal bacteria. When taken together, these results indicate that the presence of a single virus can reverse many of the abnormalities that arise in the complete absence of the commensal bacterial community (Fig. 1n).

GF mice lack bacteria from birth and represent an extreme condition. We found that adult mice treated with a cocktail of antibiotics (ABX) for 2 weeks display several of the abnormalities described above in GF mice including aberrant intestinal morphology and a reduction in the number of total $CD4^+$ Tcells as well as IFN-γ-expressing $CD4^+$ and $CD8^+$ T cells (Fig. 2a-j and Extended data Fig. 7a-d). Thus, we examined the ability of MNV infection to reverse these abnormalities induced by ABX treatment as another assay to demonstrate functional redundancies between this virus and commensal bacteria (Fig. 2a,

Extended data Fig. 1b). By day 10 post-infection, MNV.CR6 infection increased villi width, Paneth cell granules, intestinal T cells, and IFN-γ expression by $CD4^+$ T cells (Fig. 2c-m). For comparison, mice were treated with ABX for 2 weeks and then inoculated with 1×10^7 colony forming units (CFU) of representative commensals *Bacteroides thetaiotamicron* (*B. theta*), *Lactobacillus johnsonii*, or left alone after ABX removal (Extended data figure 7e-h). *B. theta* and *L. johnsonii* restored the morphology of the intestine to a similar degree as MNV.CR6, but had varying effects on the T cell compartment. *B. theta* increased T cell numbers when measured by CD3-staining of small intestinal sections while *L. johnsonii* induced an IFN-γ response in $CD4^+$ and $CD8^+$ T cells without affecting their overall numbers (Extended data Fig. 7i-p). These results are consistent with the concept that individual members of the microbiota evoke overlapping responses from the host, but are not necessarily identical.

To gain better resolution into the response evoked by MNV and commensal bacteria, we performed RNA deep sequencing analyses (RNA-seq) on whole intestinal tissue harvested from untreated GF mice, GF mice 10 days after inoculation with MNV.CR6, and GF mice reconstituted with the bacterial flora from conventional mice (Fig. 3a, Extended data table 1). Pathway analysis of the transcripts induced by commensal bacteria indicated alterations in the metabolic state, immunity, and blood vessel morphogenesis. MNV.CR6 induced a more limited gene expression pattern associated with lymphoid cell development and immune responses, many of which are related to the antiviral type I interferon (IFN-I) response (Extended data table 1a). Consistent with the shared ability of MNV and bacteria to reverse abnormalities in GF mice, the overlapping gene set contained genes associated with development and function of hematopoietic lineage cells (Fig. 3a, Extended data table 1c). The IFN-I signature induced by MNV.CR6 prompted us to examine whether the effect of viral infection was dependent on IFN-I signaling. The intestine of untreated IFNα receptor knockout mice ($IFNAR^{-/-}$) displayed a normal appearance, while ABX-treatment of these mice led to similar abnormalities in intestinal morphology and T cell numbers as described above (Fig. 3b-h). However, MNV.CR6 infection did not have a detectable effect on ABX-treated $IFNAR^{-/-}$ mice despite productive replication (Fig. 3i, Extended data fig. 1b), indicating that virus-mediated reversal of these abnormalities is dependent on IFN-I signaling. Inducing IFN-I gene expression through poly(I:C) injection was sufficient to increase villus width in GF but did not have a noticeable effect on intestinal T cells (Extended data figure 8). Thus, IFN-I signaling likely functions in conjunction with other pathways to confer the full effect of MNV infection. Indeed, transcriptional analyses supports a large overlap between the genes induced by MNV.CR6 and bacterial colonization of GF mice that are not associated with IFN-I (Extended data table 1c).

Depletion of commensal bacteria is considered a major health hazard of indiscriminate use of antibiotics. Because MNV can reverse abnormalities observed upon bacterial depletion, we tested the possibility that viral infection can provide protection against intestinal damage. We found that ABX-treatment increased sensitivity to chemical injury of the intestine by dextran sodium sulfate (DSS) (Fig. 4a). Remarkably, all three MNV strains examined were able to improve survival in ABX-treated mice receiving DSS (Fig. 4a). MNV.CR6 in particular conferred robust protection and prevented shortening of the colon (Fig. 4a, b).

MNV.CR6 was unable to improve survival in ABX-treated IFNAR$^{-/-}$ mice indicating that IFN-I signaling was necessary (Figure 4c). Next, we used inflammation induced by *Citrobacter rodentium* to test the protective effect of MNV because ABX-pretreatment was shown to exacerbate disease induced by this model enteric pathogen without altering bacterial burden[22]. In ABX-pretreated mice, MNV.CR6 did not alter the amount of *C. rodentium*, which was the dominant bacterium in the gut (Fig. 4f, Extended data fig. 9a-b). However, MNV.CR6 ameliorated weight loss, diarrhea, and histopathology (Fig. 4d-k). *C. rodentium* induces expression of virulence factors in response to host immunity and competition with other bacteria[23]. Interestingly, MNV infection of ABX-treated mice restored expression of bacterial virulence factors to levels detected in conventional mice (Extended data fig. 9c-d). This effect of the virus on bacterial gene expression and the protection from inflammation are most likely due to the ability of MNV.CR6 to enhance the immune response to *C. rodentium*, which includes increased levels of antibodies as well as antimicrobial and regulatory cytokines (Extended data fig. 9e-i). Thus, MNV enhances protection against both infectious and non-infectious secondary challenges to the gastrointestinal tract in ABX-treated animals.

RNA viruses are routinely detected in asymptomatic infants and children as well as individuals recovering from acute gastroenteritis[5, 24, 25]. Thus, in addition to periods following ABX-administration, the presence of known or unidentified viruses may be beneficial during developmental or recovery stages when the immune system and the intestinal microbiota are vulnerable. However, like bacteria, whether a given intestinal virus is a mutualist is likely to depend on host factors and the specific viral strain in question. For instance, production of IFN-I is a conserved response to viral infections, but the role of this cytokine in the gut is highly contextual and dependent on other soluble factors[26]. For this reason, it may not be surprising that MNV can protect ABX-treated mice from intestinal injury, but exacerbates disease in mice that are genetically susceptibility to IBD[15, 27]. We speculate that viruses that contribute to the pathogenesis of complex inflammatory disorders could be commensal in nature rather than exclusively pathogenic. Taken together, we demonstrate that an enteric animal virus can function in a manner analogous to commensal bacteria, and propose that symbiotic viruses exist in the mammalian gastrointestinal tract. We suggest that the incredible advances in viral discovery pipelines[28] be leveraged to discover commensal or mutualistic viruses that constitute the virome in addition to traditional pathogens.

Methods

Mice

Germfree (GF) mice on a C57BL/6J background were bred and housed in flexible film isolators in the New York University School of Medicine Gnotobiotics Animal Facility[29]. Absence of fecal bacteria and fungi was confirmed by aerobic culture in brain heart infusion, sabaraud, and nutrient broth (Sigma) and qPCR for bacterial 16S (UniF340 5′-ACTCCTACGGGAGGCAGCAGT-3′; UniR514 5′-ATTACCGCGGCTGCTGGC-3′) and eukaryotic 18S ribosomal RNA genes (B2F 5′-ACTTCGATGGTAGGATAG-3′; B4R 5′-TGATCGTCTTCGATCCCCTA-3′) through sampling of stool from individual cages in

each isolator on a monthly basis. Mono-association with MNV as described in Extended data figure 1 was performed within a dedicated isolator by inoculating 3 male and 3 female GF mice with 3×10^6 plaque forming units (pfu) of MNV.CR6 from an endotoxin-free stock prepared as described below. MNV mono-associated GF mice (GF+MNV) were bred to each other (F_0 generation), and successful transmission to offspring was confirmed by performing a plaque assay on stool collected from 8-10 week old adult progeny (4-5 weeks after weaning) (Extended data figure 1). Progeny (F_1) was used for experimental analyses or further breeding to generate additional mice for analyses (F_2). Absence of bacteria and fungi was confirmed as described above. Control GF mice were bred and maintained in a separate isolator free of MNV. Unless stated otherwise, GF and GF+MNV mice remained in isolators until the time of analyses.

Conventional C57BL/6J wild-type and IFNAR1$^{-/-}$ (B6.129S2-*Ifnar1*^{tm1Agt}/Mmjax) mice were purchased from Jackson Laboratories and bred onsite in a MNV and *Helicobacter*-negative specific pathogen free (SPF) animal facility. The absence of segmented filamentous bacteria (SFB) was determined by PCR (SFB736F 5′-GACGCTGAGGCATGAGAGCAT-3′; SFB844R 5′-GACGGCACGGATTGTTATTCA-3′). Age (6-9 weeks) and gender-matched mice were used in all experiments and assigned randomly to experimental groups. Sample size for animal experiments was chosen based on prior data generated in the laboratory. All animal studies were performed according to protocols approved by the NYU School of Medicine Institutional Animal Care and Use Committee (IACUC).

Antibiotics and DSS treatment

Mice were gavaged with 100 mg streptomycin (Sigma) and the drinking water was immediately replaced with filter-sterilized water containing ampicillin (1 g/L; American bioanalytical), vancomycin (0.5 g/L; MP biomedicals), neomycin (1 g/L; Sigma), metronidazole (1 g/L, Sigma), and 1 % sucrose (Fisher). Antibiotics-containing water was replaced at least once a week. For DSS experiments, mice were given 4 % DSS (TdB consultancy) with or without the above antibiotics cocktail in their drinking water for 6 days and then received regular or antibiotics-containing drinking water for the remainder of the experiment.

MNV and bacterial inoculation

MNV.CR6 and MNV.CW3 concentrated stock was prepared as described[30]. Briefly, supernatant from 293T cells transfected with a plasmid containing the viral genome was applied to RAW264.7 cells to amplify virus production, and virions were concentrated by ultracentrifugation and resuspension in endotoxin free PBS. Concentration of stock was determined by plaque assay as previously described[31]. For indicated experiments in which adult GF mice were exposed to MNV or bacteria outside of an isolator, 6 to 8 week old GF mice were transferred to pre-assembled autoclaved cages with autoclaved food and water. Mice were infected orally by pipet with 3×10^6 plaque forming units (pfu) resuspended in 25 μl PBS or gavaged with 100 μl of a suspension of a fresh fecal pellet from a conventional C57BL/6J mouse homogenized in 1 ml PBS. *Bacteroides thetaiotomicron* VPI-5482 (*B. theta*) provided by Eric Martens (University of Michigan Medical School, Ann Arbor, MI)

was grown in peptone yeast glucose broth for 36 hours in an anaerobic chamber (Anaerobe Systems). Mice were gavaged with 100 µl of culture containing 10^6-10^7 colony forming units (cfu) and colonization was confirmed by plating stool, small intestinal tissue, and colonic tissue on bacteroides bile esculin (BBE agar, Anaerobe Systems) plates. *Lactobacillus johnsonii* was provided by Robert Jenq (Memorial Sloan Kettering Cancer Center, New York, NY) and grown in MRS broth (BD) for 16 hours under anaerobic conditions. Mice were inoculated with 100 µl of culture (10^7 cfu) and stool, small intestinal and colonic tissue was plated on MRS agar (BD) for enumeration of *L. johnsonii* infection. *Citrobacter rodentium* DBS100 was grown in LB to OD_{600} = 1, resuspended in PBS, and mice were gavaged with 100 µl containing 2×10^9 cfu. Bacterial inocula were determined by serial dilution plating on MacConkey plates. Stool samples collected on indicated days were homogenized in 1 ml PBS, serially diluted and plated on MacConkey plates for quantification of bacterial burden. Diarrhea was quantified by subtracting the stool's dry weight from its wet weight and expressing the proportion of water as a percentage of the wet weight. 100 µg Poly(I:C) (high molecular weight, InvivoGen) was injected intraperitoneally daily for 10 days starting on day 4 of ABX treatment. In cases where ABX were lifted prior to bacterial inoculation, stool samples from individual cages were collected at the last day of ABX treatment and at the endpoint of *C. rodentium*, *B. theta* or *L. johnsonii* infection, DNA was extracted and qPCR was performed for the 16S genes of following bacterial groups: Lactobacilli (Fwd 5′-AGCAGTAGGGAATCTTCCA-3′, Rev 5′-CACCGCTACACATGGAG-3′), Enterobacteriacea (Uni515F 5′-GTGCCAGCMGCCGCGGTAA-3′; Ent826R 5′-CCTCAAGGGCACAACCTCCAAG-3′), Fusobacterium (Fwd 5′-CTAACGCGATAAGTAATC-3′, Rev 5′-TGGTAACATACGATAGGG-3′), *Bacteroides* (Fwd 5′-GAGAGGAAGGTCCCCCAC-3′, Rev 5′-CGCTACTTGGCTGGTTCAG-3′) and *C. rodentium* (Fwd 5′-AGGCCTTCGGGTTGTAAAGT-3′, Rev 5′-ATTCCGATTAACGCTTGCAC-3′).

Microscopy

Small intestinal, colonic, and cecal tissue was prepared for staining as previously described[15]. Hematoxylin and eosin (H&E) and anti-CD3 staining were performed by the NYU Histopathology core and NYU IHC core, respectively. Lysozyme staining of small intestinal sections was performed as described[32]. At least 50 villi per mouse were measured for villi width at the base of the villi where they meet the crypt or were analyzed for number of $CD3^+$ cells. Paneth cell granules were counted in at least 30 crypts per mouse. Mean values were calculate for each mouse and used as individual data points. Sections were imaged on a Zeiss Axioplan microscope. All analyses of slides were performed blind and quantified using Image J software. The histopathology score for individual mice is the sum of three parameters, including villus hyperplasia and crypt architectural distortion, degree of inflammation and edema thickness in the lamina propria and submucosa. The scoring criteria are as follows: villus hyperplasia and crypt architectural distortion: 0 = no, 1 = mild, 2 = moderate, 3 = severe; inflammation: 0 = no, 1 = focal, 2 = multifocal, 3 = transmural; edema thickness: 0 = 0 µm, 1 = 1-100 µm, 2 = 101-200 µm, 3 = 201-300 µm giving a maximal score of 9. The mean of the score for individual mice was calculated. Blind histopathology scoring was performed by a pathologist (Y.D.).

Flow cytometry

Small intestinal or colonic tissue was flushed with PBS, fat and Peyer's patches were removed and the tissue was incubated in HBSS with 5 mM EDTA and 1mM DTT at 37 °C for 20 minutes, followed by HBSS and 5 mM EDTA for 10 minutes. The tissue was digested using collagenase (Sigma) for 30 minutes, followed by a Percoll (Fisher) gradient centrifugation using 40 % and 80 % Percoll. Single cell suspensions of mesenteric lymph nodes (MLN) were prepared by passing MLNs through 100 μm cell strainers (BD) and subsequent resuspension in PBS. Total cell numbers per ml were determined by counting recovered cells in a hemocytometer. For intracellular cytokine staining, cells were stimulated using the eBioscience cell stimulation cocktail for 4 hours at 37 °C. Cells were fixed and permeabilized using the Biolegend fixation and permeabilization buffers. Samples were stained with a fixable live dead stain (Invitrogen) and live gating was performed prior to any other gating for all samples. The following antibodies (clones) were used for staining: CD4 (GK1.5), CD8 (53-6.7), CD3 (145-2C11), CD11b (M1/70), TCRβ (H57-597), Tbet (4B10), IFN-γ (XMG1.2), IL-17 (TC11-18H10.1), CD19 (6D5), Fc block (TruStainfcx) all from Biolegend; GATA3 (L50-823) from BD bioscience and IL-22 (1H8PWSR), IL-13 (eBio13A), B220 (RA3-6B2) from eBioscience. The NIH tetramer facility provided the mCD1d tetramer. FlowJo version 10 was used to analyze flow cytometry data.

RNA sequencing

RNA was extracted from 2 cm of snap frozen small intestinal tissue with TriZol reagent (Fisher Bioscience) using manufacturer protocol. RNA library was prepared using the Illumina TruSeq RNA sample preparation kit and sequenced with the Illumina Hiseq2000 using the TruSeq RNA v2 protocol. Illumina CASAVA version 1.8.2 was used to generate FASTQ files containing 29.5-53.5 M qualified reads per sample. Alignment and gene expression count were computed using default settings, which aligns reads to the union of all RefSeq-annotated exons for each gene. 59% to 78% of reads were aligned to mouse genome version mm9. All genes expressed below one base pair per million (cpm) in the majority of replicates in all treatments have been filtered from the data set. The Bioconductor package edgeR was used to find differentially expressed genes with FDR below 5%[33]. Sequencing data have been submitted to GEO (accession number GSE60163). The DAVID (Database of Annotation, Visualization and Integrated Discovery) bioinformatics resource was used to assign differentially regulated genes to Gene Ontology functional categories and determine enrichment scores and significance by a modified Fisher Exact test[34]. Gene set enrichment analysis (GSEA, Broad institute) analysis was performed in Gene Pattern using the GSEA_Preranked module and a Geneset file created by the Bader lab for mouse (http://download.baderlab.org/EM_Genesets/current_release/Mouse/Entrezgene) with RNA-seq gene expression results ranked by fold change of MNV treated vs Uninfected and of Conventional vs. Uninfected.

ELISA

2 cm of small intestinal tissue was homogenized in 1 ml PBS containing protease inhibitor cocktail or serum was collected. Samples were diluted 1:100 and levels of IgA and IgG2c (ng/ml) were determined according to the manufacturer' protocol (Southern Biotech).

Isolation of MNV from vivarium

Stool from Rag1$^{-/-}$ mice housed in an MNV-positive room within the Skirball vivarium was tested for presence of MNV with previously described primers and nested PCR condition[35]. Stool from the same mice was homogenized in 1 ml of DMEM, and the supernatant was cleared by centrifugation and filtered through a 0.2 μm filter. 50 μl were added to a well of RAW264.7 cells seeded in a 6 well dish. Five days later the cells and supernatant were harvested, freeze-thawed and transferred to a 10 cm dish of RAW264.7 cells for amplification. After another 5 days, virus in supernatant was concentrated by ultracentrifugation. For phylogenetic analysis RNA was isolated using Trizol and standard protocols and cDNA was prepared with ProtoScript M-MuLV First Strand cDNA synthesis kit (New England Biolabs) and random hexamers. The capsid region was amplified and sequenced as previously described[36]. Capsid sequences from various MNV strains were aligned using Clustal Omega (EMBL-EBI). The sequence of the capsid region was deposited to the NCBI database under the designation MNV SKI (accession number KM463105).

qRT-PCR

Total RNA from colonic tissue was isolated using Trizol and standard protocols, followed by cDNA synthesis using ProtoScript M-MuLV First Strand cDNA synthesis kit (New England Biolabs) and OligodTs. qPCR was performed on a Roche480II Lightcycler using the following primers: Gbp2 (Fwd 5′-TGCTAAACTTCGGGAACAGG-3′, Rev 5′-GAGCTTGGCAGAGAGGTTTG-3′), IL-10 (Fwd 5′-GCCGTCATTTTCTGCCTCAT-3′; Rev 5′-GCTTCCCTATGGCCCTCATT-3′), IFN-γ (Fwd 5′-ATGAACGCTACACACTGCATC-3′; Rev 5′-CCATCCTTTTGCCAGTTCCTC-3′), Gapdh (Fwd 5′-TGCCCCCATGTTTGTGATG-3′, Rev 5′-TGTGGTCATGAGCCCTTCC-3′). Relative expression of the respective genes to Gapdh expression was calculated using the ΔΔCt method and values were expressed as fold change from ABX treated mice. Total RNA from stool was isolated with Trizol followed by cDNA synthesis with random hexamer primers for quantification of *C. rodentium* virulence factor expression with the following primers ler (Fwd 5′-AATATACCTGATGGTGCTCTTG-3′, Rev 5′-TTCTTCCATTCAATAATGCTTCTT-3′), tir (Fwd 5′-TACACATTCGGTTATTCAGCAG-3′, Rev 5′-GACATCCAACCTTCAGCATA-3′) and recA (Fwd 5′-CGCATTCGCTTTACCCTGACC-3′, Rev 5′-TCGTCGAAATCTACGGACCGGA-3′).

Statistical analysis

Analyses except for RNA-seq data used Graphpad Prism version 6. An unpaired two-tailed t test was used to evaluate differences between two groups where data was distributed normally with equal variance between conditions. An ANOVA with Holm-Sidak multiple comparisons test was used to evaluate experiments involving multiple groups. The log rank Mantel Cox test was used for comparison of mortality curves.

Europe PMC Funders Author Manuscripts

Extended Data

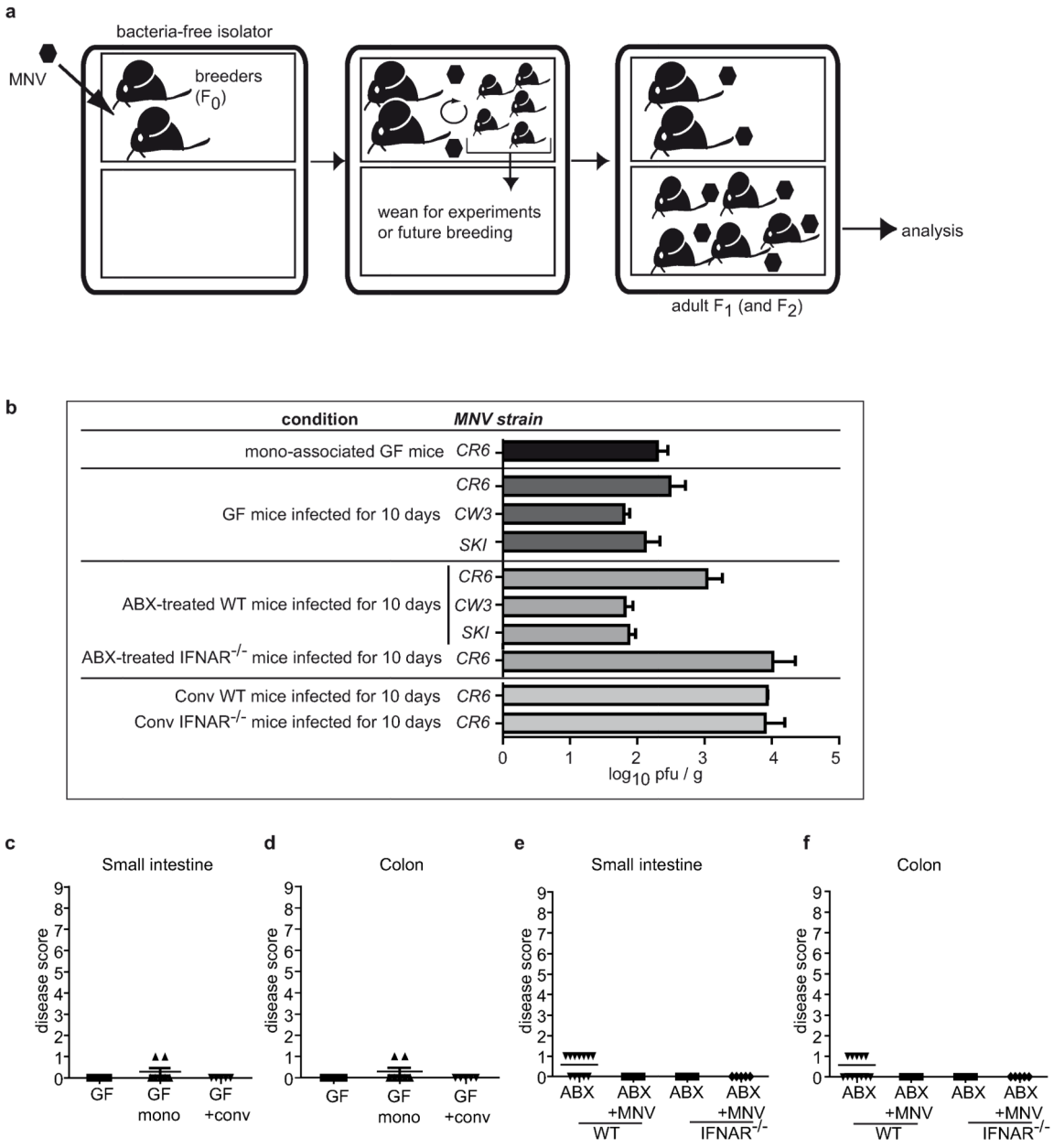

Extended data figure 1. Mono-association of germfree mice with MNV does not lead to uncontrolled viral replication or disease

(a) Schematic of MNV mono-association procedure (see methods for additional details). Germfree (GF) breeder pairs (F_0) within a gnotobiotic isolator were infected with 3×10^6 plaque forming units (pfu) of MNV.CR6, which was allowed to transmit naturally to offspring (F_1). Weaned offspring were maintained in isolators until adulthood, and then either used for analysis or as breeders to generate additional experimental animals (F_2). **(b)** Successful transmission to offspring and the persistent presence of the virus in mono-associated GF mice (GF+MNV) was confirmed by performing a plaque assay using stool

harvested from 8 week old offspring (~1 month after weaning). The amount of virus in stool from GF mice, antibiotics (ABX)-treated WT and IFNAR$^{-/-}$ mice, and conventional (Conv) mice infected with 3×10^6 pfu of the indicated strains of MNV for 10 days are also shown, N = 5 mice per group. **(c-f)** Mice receiving the indicated treatments did not display significant histopathology in the small intestine (c,e) and colon (d,f) based on blind quantification of H&E-stained sections using a previously described scoring system[37]. Mice receiving a pathology score of 1 displayed mild blunting of villi (additional details in Methods section). No histopathology was detected in spleens, and no other signs of disease were noted. Note that a previous publication in which mice were reported to display pathologies following MNV infection used a different strain of MNV, an early time point (24 hours post-infection), and mice on a different background (129/Sv) [38]. The lack of pathology in C57BL/6 mice persistently infected with MNV.CR6 is consistent with our previous publication[15]. N = 5-7 mice/group. *$p<0.05$; **$p<0.01$. All graphs display means ± SEM.

Europe PMC Funders Author Manuscripts

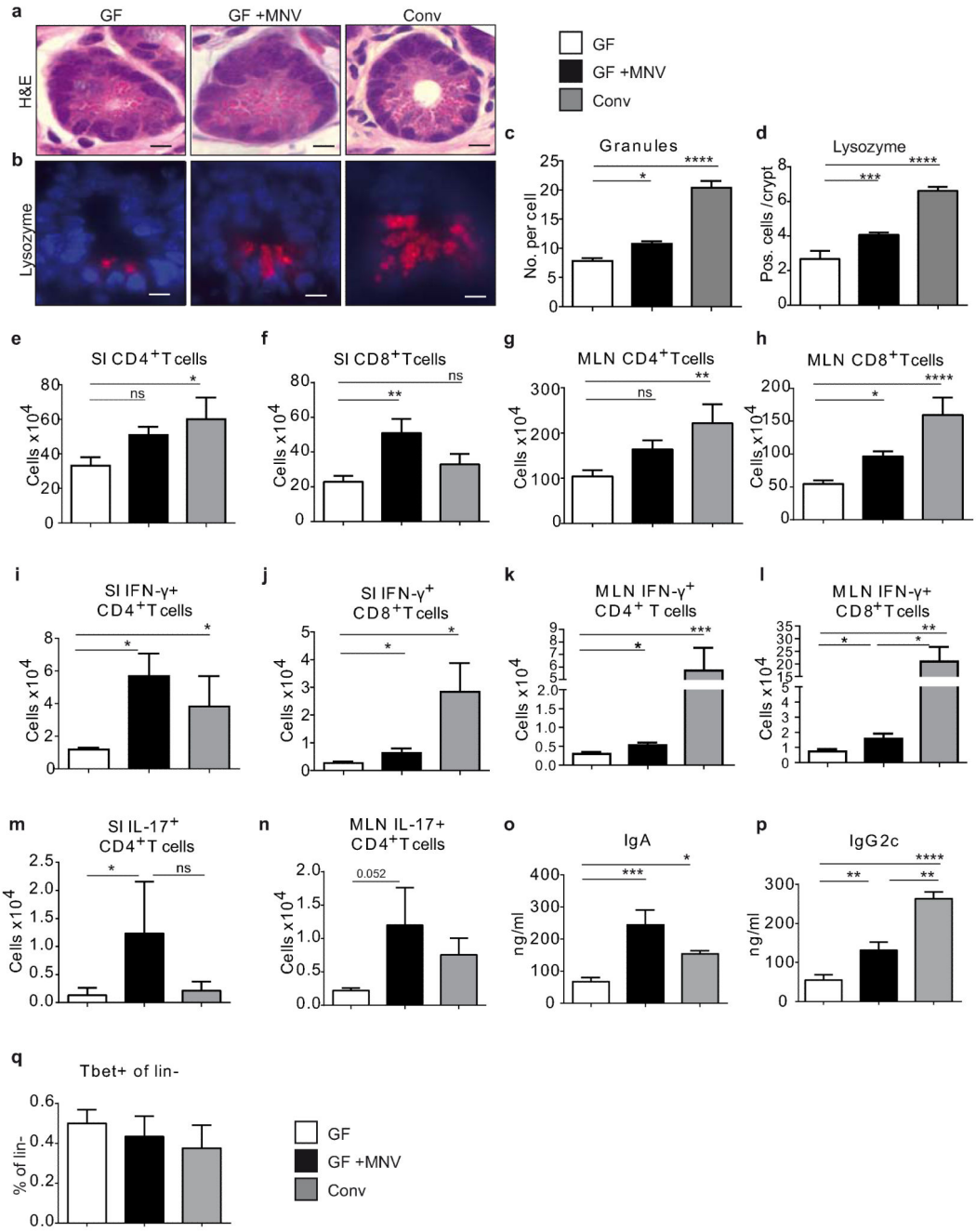

Extended data figure 2. MNV improves several deficiencies related to intestinal immunity in germfree mice

(a,b) Representative images of crypts from small intestinal tissue sections stained with H&E (a) and an anti-lysozyme antibody (b) harvested from GF, GF+MNV (mono-association), and Conv mice. Scale bar represents 1 μm. **(c,d)** Quantification of the above images show an increase in granules per Paneth cell (c) and lysozyme positive cells per crypt (d) in GF +MNV mice, indicating that the presence of MNV partially reverses Paneth cell abnormalities due to the absence of bacteria. N = 5 mice/group. **(e-h)** MNV mono-association of GF mice increases the number of $CD4^+$ (e,g) and $CD8^+$ (f,h) T cells ($TCR\beta^+$)

Europe PMC Funders Author Manuscripts

in small intestinal (SI) lamina propria (LP) and mesenteric lymph nodes (MLN). **(i-n)** Flow cytometry analysis indicates that MNV mono-association of GF mice also increases the number of IFN-γ expressing $CD4^+$ and $CD8^+$ T cells in SI LP (i,k) and MLN (j,l). IL-17 expression by CD4+ T cells is also influenced by the presence of MNV (m,n). N = 10 **(o,p)** GF+MNV mice display increased IgA levels in SI tissue (o) and IgG2c levels in serum (p). N = 5 mice per group. **(q)** Percentage of T-bet^+ cells in the SI LP after gating on live and lin^- cells remain unchanged by MNV infection of GF mice. N = 10 mice/group. ns = not significant; *p<0.05; **p<0.01; ***p<0.001, ****p<0.0001. All graphs display means ± SEM from at least two independent experiments

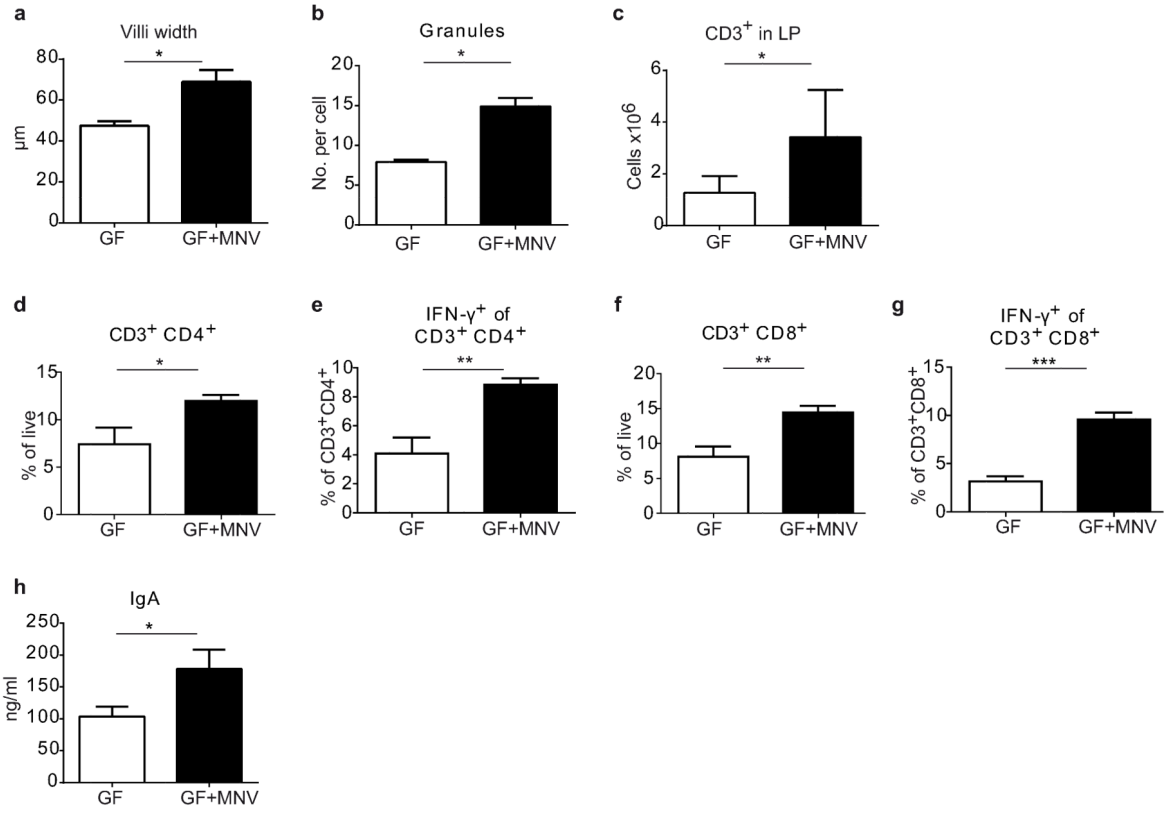

Extended data figure 3. MNV infection of adult germfree mice has similar effects as mono-association of germfree mice from birth

6-8 week old adult GF mice were infected with MNV.CR6 for 10 days and examined for reversal of intestinal abnormalities. **(a,b)** Quantification of villi width (a) and granules per Paneth cell (b) in H&E-stained small intestinal sections. N = 5 mice/group. **(c)** Quantification of the number of $CD3^+$ T cells in the SI LP by flow cytometric analysis. N = 6 mice/group. **(d, e)** Quantification of IFN-γ producing $CD3^+CD4^+$ (d) and $CD3^+CD8^+$ (e) T cells by flow cytometry. **(f)** Quantification of small intestinal IgA by ELISA. N = 6 mice/group. *p<0.05. All graphs display means ± SEM from at least two independent experiments.

Europe PMC Funders Author Manuscripts

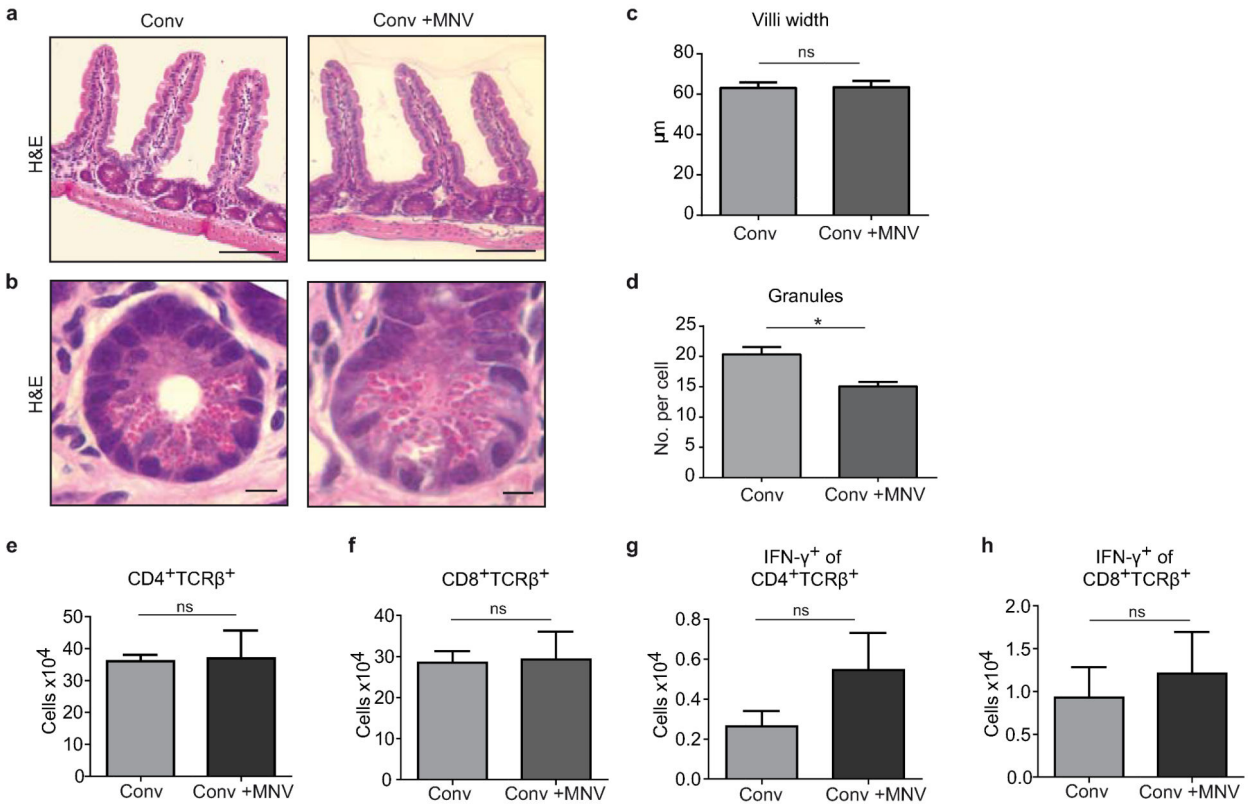

Extended data figure 4. The effect of MNV is specific to mice depleted of bacteria

Conv mice were infected with 3×10^6 pfu of MNV.CR6 to determine the effect of MNV in the presence of commensal bacteria. **(a,b)** Representative images of H&E-stained small intestinal sections of Conv and Conv+MNV mice showing no aberrant changes after MNV infection. Scale bar represents 100 μm in (a) and 1 μm in (b). **(c,d)** Villi width (c) and Paneth cell granules (d) were quantified from at least 50 villi and 30 crypts of 2-5 mice per group. **(e-h)** Cell numbers of $CD4^+TCR\beta^+$ (e), $CD8^+TCR\beta^+$ (f), IFN-γ producing $CD4^+$ (g), and IFN-γ producing $CD8^+$ T cells in SI LP (h). N = 6 mice/group. ns = not significant, *$p<0.05$. All graphs display means ± SEM from at least two independent experiments.

Europe PMC Funders Author Manuscripts

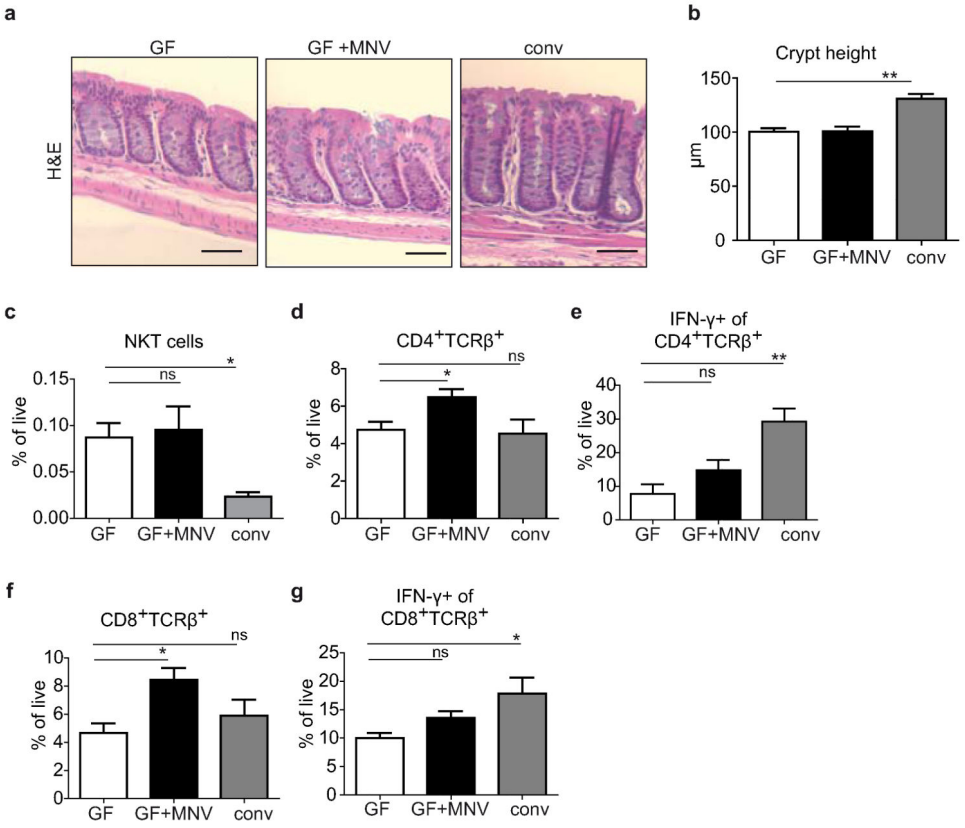

Extended data figure 5. MNV mono-association of GF mice increases colonic lymphocyte populations

(a-b) Representative images of H&E stained colonic small intestinal sections (a) of GF, GF +MNV (mono-association with MNV.CR6) and Conv mice. Scale bar represents 100 µm. (b) In above mice the crypt height was measured showing a significant difference in GF and Conv mice. **(c)** Percentages of NKT cells ($CD1d^+$, $TCR\beta^+$) in colonic lamina propria of GF, GF+MNV and conv mice. **(d-g)** Percentages of $CD4^+TCR\beta^+$ (d) and $CD8^+TCR\beta^+$ cells (f), and percentages of IFN-γ producing $CD4^+$ (e) and $CD8^+$ T cells (g) in the colonic LP of GF, GF+MNV and conv mice. ns = not significant; *p<0.05; **p<0.01. N = 5 mice/group. All graphs display means ± SEM from at least two independent experiments.

Europe PMC Funders Author Manuscripts

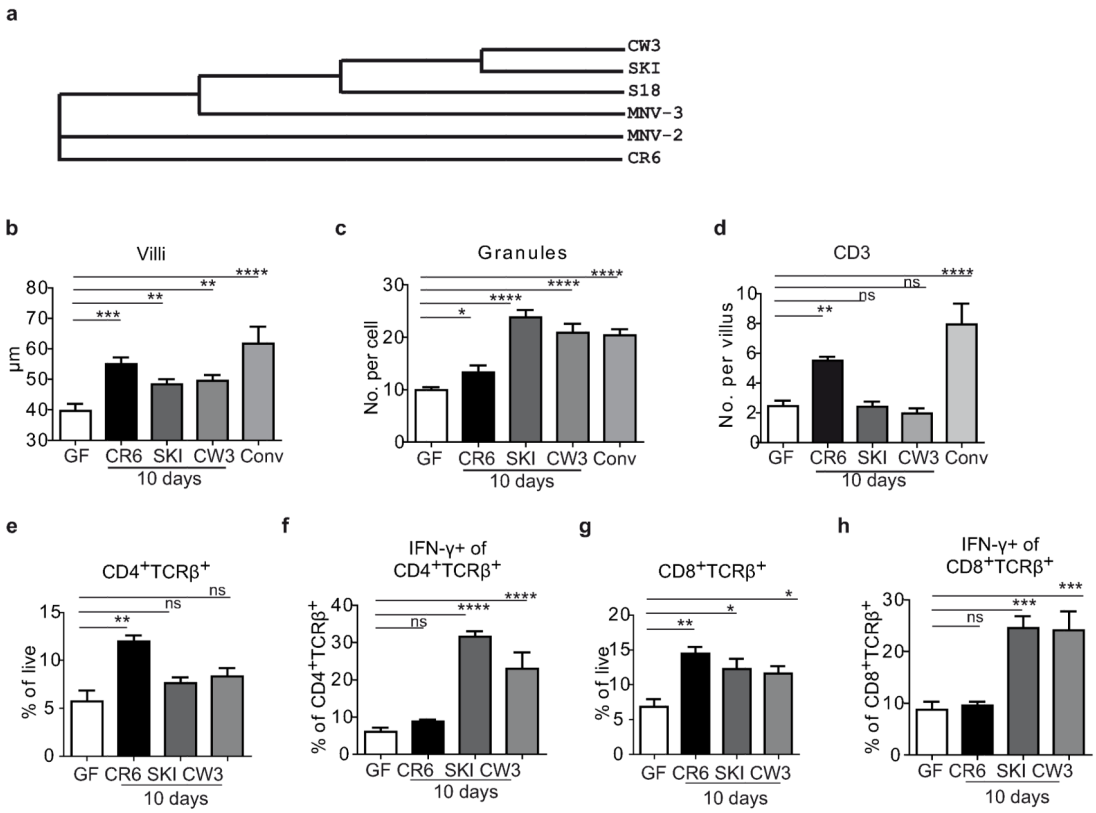

Extended data figure 6. The effect of MNV on the small intestine of GF mice is not strain specific

(a) Phylogenetic tree of the capsid sequences of indicated MNV strains. **(b-d)** Quantification of the villi width (b), granules (b) and $CD3^+$ cells (d) in small intestinal sections prepared from Conv mice, GF mice, and GF mice infected with the indicated strains of MNV for 10 days. **(e-h)** Percentages of $CD4^+TCR\beta^+$ (e) and $CD8^+TCR\beta^+$ cells (g), and percentages of IFN-γ producing $CD4^+$ (f) and $CD8^+$ T cells (h) in the SI LP of indicated mice. N = 6 mice/group. ns = not significant *p<0.05; **p<0.01; ***p<0.001, ****p<0.0001. All graphs display means ± SEM from at least two independent experiments

Europe PMC Funders Author Manuscripts

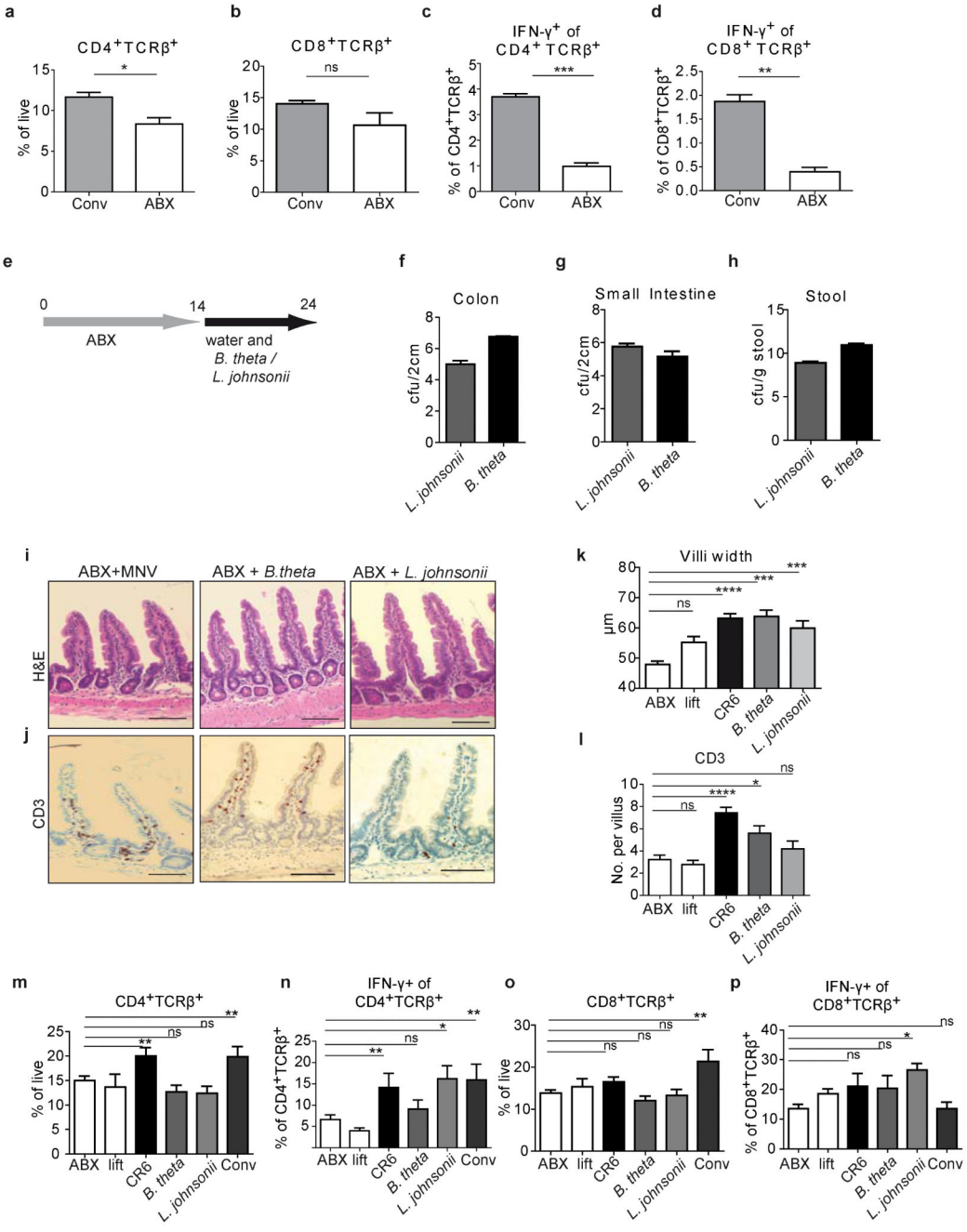

Extended data figure 7. Antibiotics treatment induces intestinal abnormalities that can be reversed by *Bacteroides thetaiotamicron*, *Lactobacillus johnsonii* or MNV.CR6

(a-g) Percentages of $CD4^+TCR\beta^+$ (a) and $CD8^+TCR\beta^+$ cells (b), and percentages of IFN-γ producing $CD4^+$ (c) and $CD8^+$ T cells (d) in SI LP in Conv mice with and without ABX. N = 5-10 mice/group. **(e)** Schematic of ABX treatment for introducing bacteria. After 14 days, ABX-containing water was replaced by regular water after 14 days. Mice were then inoculated with *Bacteroides thetaiotamicron* (*B. theta*), *Lactobacillus johnsonii* (*L. johnsonii*), or left untreated for 10 days prior to analyses. **(f-h)** Bacterial loads of colon (f),

Europe PMC Funders Author Manuscripts

small intestine (g) and stool (h) of ABX-treated mice inoculated with *B. theta* or *L. johnsonii* for 10 days. **(i,j)** Small intestinal sections stained with H&E (i) or anti-CD3 antibody (j) indicating that inoculation with MNV.CR6, *B. theta* or *L. johnsonii* have similar effects on intestinal morphology. **(k,l)** Mice that received ABX during the whole course of the experiment with or without MNV (ABX and ABX+MNV) were compared to mice treated as in (e) using the previously described measurements: quantification of villi width (k), $CD3^+$ cells per villi (l), and percentages of $CD4^+$ (m), $CD8^+$ (o), IFN-γ^+CD4^+ (n) and IFN-γ^+CD8^+ (p) T cells in the SI LP. N = 8 mice/group. ns: not significant, *p<0.05, **p<0.01, and ***p<0.001. All graphs display means ± SEM from at least two independent experiments.

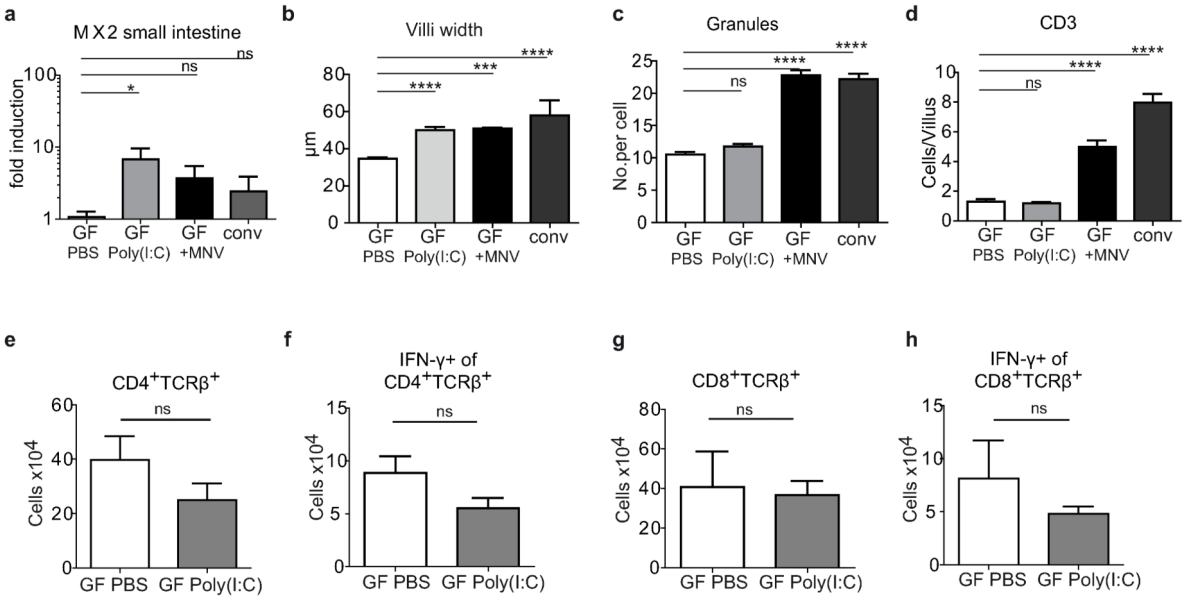

Extended data figure 8. Type I interferon induction by Poly(I:C) changes small intestinal architecture without affecting the T cell compartment

(a) qRT-PCR quantification of the type I interferon (IFN-I) inducible gene *MX2* in small intestinal tissue of untreated GF mice, GF mice injected for 10 days with Poly(I:C), MNV.CR6 mono-associated GF mice (GF+MNV), and conv mice indicate that the poly(I:C) injection procedure induces an IFN-I response. Values represent fold induction of *MX2* compared to untreated GF mice after normalizing to *Gapdh*. **(b-d)** Quantification of the villi width (b), granules (c) and $CD3^+$ cells in the small intestine of same mice of H&E stained small intestinal sections. **(e-h)** Percentages of $CD4^+TCR\beta^+$ (e), $CD8^+TCR\beta^+$ cells (g), and IFN-γ producing $CD4^+$ (f) and $CD8^+$ (h) T cells from the SI LP. N = 6 mice/group. ns = not significant, ***p<0.001, and ****p<0.0001. All graphs display means ± SEM from at least two independent experiments.

Europe PMC Funders Author Manuscripts

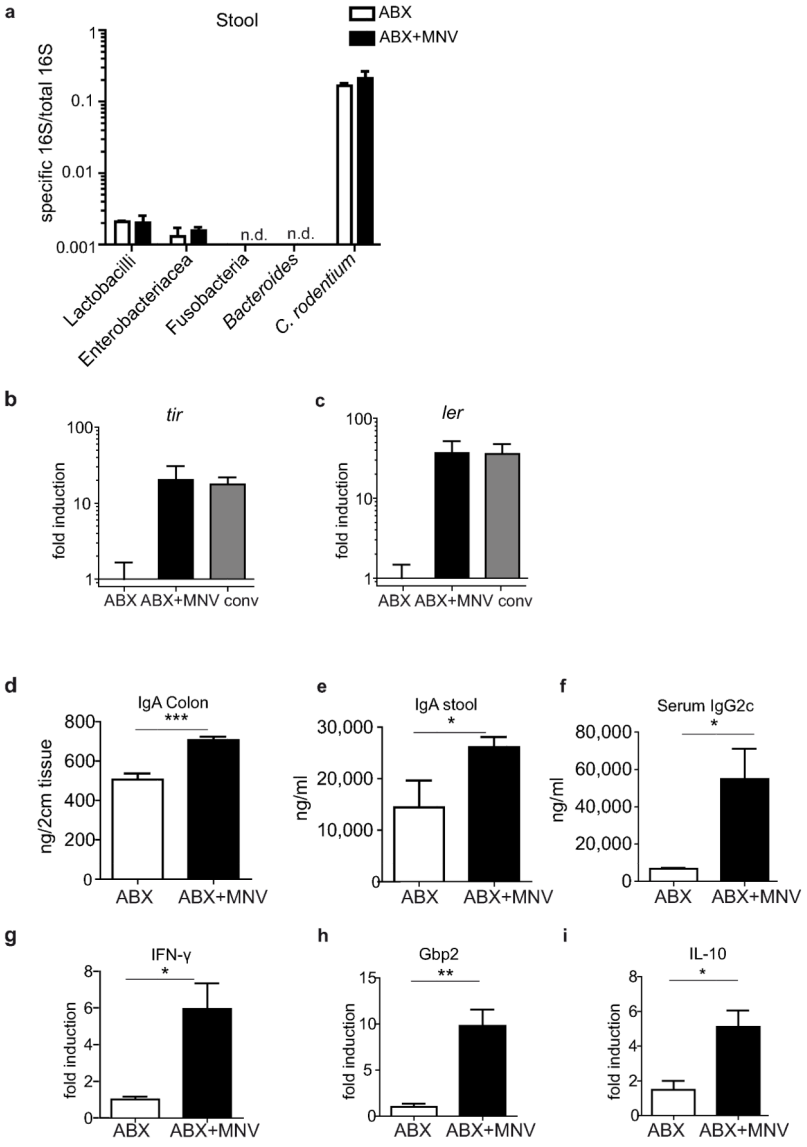

Extended data figure 9. MNV infection alters the host response to a super infection with *C. rodentium*

(a) Taxon-specific 16S qRT-PCR for Lactobacilli, Enterobacteriacea, Fusobacteria, *Bacteroides* and *C. rodentium* normalized to total 16S gene expression in stool of mice infected for 9 days with *C. rodentium* after ABX pretreatment with or without MNV.CR6 infection showing similar colonization of mice throughout the groups. **(b-c)** Fold induction of *C. rodentium* virulence factors *tir* (b) and *ler* (c) compared to the ABX group after normalization to *recA* in stool of indicated mice on day 9 post *C. rodentium* infection. **(d-f)** MNV.CR6 infection of ABX-treated mice prior to *C. rodentium* infection increases IgA levels in colonic tissue (d), stool (e), and IgG2c levels in serum (f) at day 9 post *C. rodentium* infection. **(g-i)** At day 9 post *C. rodentium* infection, ABX+MNV mice display elevated expression of IFN-γ (g), Gbp2 (h), and IL-10 (i) in colonic tissue compared to ABX

Europe PMC Funders Author Manuscripts

mice. N = 5 mice/group. ns = not significant, *p<0.05, **p<0.01, and ***p<0.001. All graphs display means ± SEM from at least two independent experiments.

Europe PMC Funders Author Manuscripts

Europe PMC Funders Author Manuscripts

Extended data table 1

Genes displaying increased expression after MNV infection or conventionalization of germfree mice

Genes upregulated more than 1.4 fold in the RNAseq experiment have been subjected to DAVID pathway analysis (Fig. 3) which assigned genes to GO (gene ontology) categories. **(a-c)** Individual genes are shown with their GO category for GF+MNV (a), for conventionalized GF (GF+conv) mice (b) or overlapping genes of the GF+MNV and GF+conv condition (c). **(d)** The same data set was analyzed using GSEA analysis, NES = normalized enrichment score.

a >1.4 fold upregulated in GF+MNV compared to GF

Term	*pValue*	Genes
immune response	***7.15E-10***	CSF2, MBL2, IFIH1, TBK1, TNFSF15, CXCL9, OAS3, RSAD2, IL15, SP110, OAS2, TLR7, CCL4,CXCL10, B2M, KLHL6, CCL20, LOC547349, PGLYRP2, OASL2, OASL1, BCL6,MX1, MX2, LTB, DHX58, GBP8, ICOSL, GBP6, IGJ, LAT, IL18BP, LAX1, CXCL13, SERPINA3G, IRF7, VEGFA, H2-OB, OAS1B, CD79B, OAS1A, H2-T24, OAS1G, OAS1E
positive regulation of immune system processes	***1.18E-05***	MBL2, ITGAL, ICOSL, IL27RA, IKZF1, TBK1, CD247, PTPN22, IL15, TNFRSF4, B2M, CDKN1A, CORO1A, CD37, CD19, KLHL6, LAX1, LCK, BCL6, CD79B, SASH3
sodium ion transport	***1.20E-05***	SLC12A6, ATP1B1, SLC5A1, ATP1A1, SLC10A5, SLC10A2, TRPM2, SLC23A1, CATSPER4, SLC4A10, SLC6A8, SLC5A4A, SLC5A8, SLC13A1, SLC13A2, SLC5A12
defense response	***6.90E-04***	MBL2, IFIH1, IL27RA, TBK1, CRP, CXCL9, RSAD2, SP110, TLR7, CCL4, TNFRSF4, LEAP2,CXCL10, B2M, SERPINA1B, CCL20, KLKB1, PGLYRP2, CLEC2H, MX1, MX2, DHX58, B4GALT1, BMP2, LIPA, MAP2K3, LAT, HIF1A, CXCL13
response to virus	***7.39E-04***	PLSCR1, IFIH1, ISG15, IRF7, OAS1B, RSAD2, OAS1A, MX1, MX2, TLR7
antigen receptor mediated signaling pathway	***9.40 E-04***	KLHL6, CD19, LAX1, CD247, LCK, PTPN22, CD79B
immune system development	***1.48E-03***	CSF2, ICOSL, EPAS1, IKZF1, SLC37A4, PTPN22, ZBTB16, SOX6, IL15, PLSCR1, DOCK2, HIF1A, CXCL13, MFSD7B, LCK, VEGFA, BCL6, JAK2, HEP
hemopoietic or lymphoid organ development	***1.99E-03***	CSF2, EPAS1, IKZF1, SLC37A4, PTPN22, ZBTB16, IL15, SOX6, PLSCR1, DOCK2, HIF1A, CXCL13, MFSD7B, LCK, VEGFA, BCL6, JAK2, HEPH, LTB, RHOH

b >1.4 fold upregulated in GF+conv compared to GF

Term	*pValue*	Genes
carboxylic acid transport	***2.12E-06***	SLC27A1, SLC36A1, SLC7A15, PPARD, SLC38A8, XK, SLC7A10, CACNB4,SLC6A18, SLC10A2, SLC19A1, SLC7A14, SLC6A9, SLC26A6, SLC6A8, SLC25A22, SLC27A2, SLC43A1, SLC46A1
amino acid transport	***5.06E-05***	SLC36A1, SLC7A15, SLC38A8, SLC7A10, XK, CACNB4, SLC19A1, SLC6A18, SLC7A14, SLC6A9, SLC6A8, SLC25A22, SLC43A1, SLC46A1
glucose transport	***5.33E-05***	PRKAG3, SLC2A8, G6PC, SLC2A3, SLC2A2, SLC5A1, EDN1, SLC37A4, KLF15
response to hypoxia	***7.70E-05***	ATP1B1, EPAS1, IL18, EDN1, BNIP3, TRF, CITED2, SLC2A8, VEGFA, P2RX2, HIF3A, NOS2, LCT
enzyme linked receptor protein signaling pathway	***7.15E-04***	FGFR1, WFIKKN2, EID2, NOG, ERBB3, SLC2A8, EIF4EBP1, FRS3, PDGFC, SH2B2, SKIL, INSR, FIGF, NR1H3, TXNIP, RET, IRS2, SMAD9, SMAD7, SMAD4, TAB1, EPHA1, NTRK3, CSRNP1, VEGFA, NTRK2, TGFBR3, HPGD
vitamin A metabolic process	***1.61E-03***	RDH9, RBP4, PPARD, LRAT, DHRS9, RDH16, BCO2

Europe PMC Funders Author Manuscripts

b >1.4 fold upregulated in GF+conv compared to GF

Term	*pValue*	Genes
acute inflammatory response	***2.53E-03***	REG3B, ORM1, C3, CFB, EPHX2, VNN1, CFI, REG3G, CFD, TRF, CD163, C8G
blood vessel morphogenesis	***2.62E-03***	FGFR1, EPAS1, EGFL7, SMAD7, IL18, EDN1, CDH2, CITED2, APOB, HEY1, HAND2, NTRK2, NOTCH4, VEGFA, PLCD3, RHOB, SOX18, NOS3, NOS2, SOX17, FIGF

c >1.4 fold upregulated common genes

Term	*pValue*	Genes
glucose transport	***2.14E-04***	PRKAG3, SLC2A2, SLC5A1, SLC37A4, KLF15
erythrocyte differentiation	***0.00172446***	EPAS1, VEGFA, BCL6, HEPH, SOX6
steroid metabolic process	***0.00176271***	RDH9, HSD3B3, APOA1, OSBPL3, HMGCS2, OSBPL1A, SLC37A4, SULT2B1
hemopoiesis	***0.00573704***	EPAS1, SLC37A4, VEGFA, PTPN22, BCL6, HEPH, IL15, SOX6, ZBTB16
homeostasis of number of cells	***0.00742149***	EPAS1, SLC37A4, VEGFA, BCL6, HEPH, SOX6
immune system development	***0.01097433***	EPAS1, SLC37A4, VEGFA, PTPN22, BCL6, HEPH, IL15, SOX6, ZBTB16
oxidation reduction	***3.14E-04***	ACOX2, BCMO1, HSD3B3, PTGR1, CYP3A13, CYP2C44, CYP3A11, CYP4V3, MOSC1, KMO, BBOX1, RDH9, AKR1B7, CYP27A1, HEPH, RDH16, CYP2C38, MOSC1, KMO, BBOX1, RDH9, AKR1B7, CYP27A1, HEPH, RDH16, CYP2C38, HPGD, CYP3A44
myeloid cell differentiation	***0.0198445***	EPAS1, VEGFA, BCL6, HEPH, SOX6

d GF+MNV vs GF	NES	GF+conv vs GF	NES
TCR	5.162	membrane trafficking	4.713
EGFR1	5.079	endocytosis	3.828
cytokine signaling in immune system	4.961	signaling by NGF	3.612
class I MHC mediated antigen processing and presentation	4.642	EGFR1	3.525
BCR	3.897	transport to the Golgi and subsequent modification	3.067
interferon gamma signaling	3.883	platelet homeostasis	3.050
growth hormone receptor signaling	3.730	PPAR signaling pathway	3.045
IL12-mediated signaling events	3.675	growth hormone receptor signaling	3.023
ER-phagosome pathway	3.622	cell-cell communication	2.987
chemokine signaling pathway	3.619	hemostasis	2.930
costimulation by the CD28 family	3.562	trans-golgi network vesicle budding	2.923
signaling by NGF	3.528	integration of energy metabolism	2.385
T cell receptor signaling pathway	3.525	MAPK signaling pathway	2.285
CXCR4-mediated signaling events	3.350	IL6	2.202

Supplementary Material

Refer to Web version on PubMed Central for supplementary material.

Acknowledgments

We would like to thank Sergei Koralov and P'ng Loke for advice on the manuscript, Elisa Venturini of the NYU Genome Technology Center for assistance with deep sequencing, Stuart Brown and Zuojian Tang of Center for Health Informatics and Bioinformatics for data analysis, Luis Ciriboga of the immunohistochemistry core for CD3 staining, the flow cytometry and histopathology cores (Cancer Center Support Grant, P30CA016087) for assistance with sample preparation and analyses, and Margie Alva of the Gnotobiotics Animal Facility (Ralph S. French Charitable Foundation) and Dan Littman for assistance with breeding and maintaining germfree mice, and Hernandez Moura Silva for sample collection for MNV isolation. This research was supported by NIH grant R01 DK093668 (K.C.), New York University Whitehead Fellowship (K.C.), Vilcek Fellowship (E.K.), and Erwin Schrödinger Fellowship from the Austrian Science Foundation (FWF) (E.K.).

References

1. Honda K, Littman DR. The microbiome in infectious disease and inflammation. Annu Rev Immunol. 2012; 30:759–95. [PubMed: 22224764]
2. Duerkop BA, Hooper LV. Resident viruses and their interactions with the immune system. Nat Immunol. 2013; 14:654–9. [PubMed: 23778792]
3. Virgin HW. The Virome in Mammalian Physiology and Disease. Cell. 2014; 157:142–150. [PubMed: 24679532]
4. Norman JM, Handley SA, Virgin HW. Kingdom-agnostic Metagenomics and the Importance of Complete Characterization of Enteric Microbial Communities. Gastroenterology. 2014; 146:1459–69. [PubMed: 24508599]
5. Donaldson EF, Lindesmith LC, Lobue AD, Baric RS. Norovirus pathogenesis: mechanisms of persistence and immune evasion in human populations. Immunol Rev. 2008; 225:190–211. [PubMed: 18837783]
6. Popgeorgiev N, Temmam S, Raoult D, Desnues C. Describing the silent human virome with an emphasis on giant viruses. Intervirology. 2013; 56:395–412. [PubMed: 24157886]
7. Ninomiya M, Takahashi M, Nishizawa T, Shimosegawa T, Okamoto H. Development of PCR assays with nested primers specific for differential detection of three human anelloviruses and early acquisition of dual or triple infection during infancy. J Clin Microbiol. 2008; 46:507–14. [PubMed: 18094127]
8. Ott C, et al. Use of a TT virus ORF1 recombinant protein to detect anti-TT virus antibodies in human sera. J Gen Virol. 2000; 81:2949–58. [PubMed: 11086126]
9. Minot S, et al. The human gut virome: inter-individual variation and dynamic response to diet. Genome Res. 2011; 21:1616–25. [PubMed: 21880779]
10. Modi SR, Lee HH, Spina CS, Collins JJ. Antibiotic treatment expands the resistance reservoir and ecological network of the phage metagenome. Nature. 2013; 499:219–22. [PubMed: 23748443]
11. Reyes A, et al. Viruses in the faecal microbiota of monozygotic twins and their mothers. Nature. 2010; 466:334–8. [PubMed: 20631792]
12. Handley SA, et al. Pathogenic simian immunodeficiency virus infection is associated with expansion of the enteric virome. Cell. 2012; 151:253–66. [PubMed: 23063120]
13. Karst SM, Wobus CE, Lay M, Davidson J, Virgin H.W.t. STAT1-dependent innate immunity to a Norwalk-like virus. Science. 2003; 299:1575–8. [PubMed: 12624267]
14. Wobus CE, et al. Replication of Norovirus in cell culture reveals a tropism for dendritic cells and macrophages. PLoS Biol. 2004; 2:e432. [PubMed: 15562321]
15. Cadwell K, et al. Virus-plus-susceptibility gene interaction determines Crohn's disease gene Atg16L1 phenotypes in intestine. Cell. 2010; 141:1135–45. [PubMed: 20602997]
16. Round JL, Mazmanian SK. The gut microbiota shapes intestinal immune responses during health and disease. Nat Rev Immunol. 2009; 9:313–23. [PubMed: 19343057]

17. Kuss SK, et al. Intestinal microbiota promote enteric virus replication and systemic pathogenesis. Science. 2011; 334:249–52. [PubMed: 21998395]
18. Kane M, et al. Successful transmission of a retrovirus depends on the commensal microbiota. Science. 2011; 334:245–9. [PubMed: 21998394]
19. Olszak T, et al. Microbial exposure during early life has persistent effects on natural killer T cell function. Science. 2012; 336:489–93. [PubMed: 22442383]
20. Thackray LB, et al. Murine noroviruses comprising a single genogroup exhibit biological diversity despite limited sequence divergence. J Virol. 2007; 81:10460–73. [PubMed: 17652401]
21. Mortha A, et al. Microbiota-dependent crosstalk between macrophages and ILC3 promotes intestinal homeostasis. Science. 2014; 343:1249288. [PubMed: 24625929]
22. Wlodarska M, et al. Antibiotic treatment alters the colonic mucus layer and predisposes the host to exacerbated Citrobacter rodentium-induced colitis. Infect Immun. 2011; 79:1536–45. [PubMed: 21321077]
23. Kamada N, et al. Regulated virulence controls the ability of a pathogen to compete with the gut microbiota. Science. 2012; 336:1325–9. [PubMed: 22582016]
24. Grohmann G, et al. Outbreak of human calicivirus gastroenteritis in a day-care center in Sydney, Australia. J Clin Microbiol. 1991; 29:544–50. [PubMed: 1645369]
25. Matson DO, Estes MK, Tanaka T, Bartlett AV, Pickering LK. Asymptomatic human calicivirus infection in a day care center. Pediatr Infect Dis J. 1990; 9:190–6. [PubMed: 2159612]
26. Gonzalez-Navajas JM, Lee J, David M, Raz E. Immunomodulatory functions of type I interferons. Nat Rev Immunol. 2012; 12:125–35. [PubMed: 22222875]
27. Basic M, et al. Norovirus triggered microbiota-driven mucosal inflammation in interleukin 10-deficient mice. Inflamm Bowel Dis. 2014; 20:431–43. [PubMed: 24487272]
28. Lipkin WI, Firth C. Viral surveillance and discovery. Curr Opin Virol. 2013; 3:199–204. [PubMed: 23602435]

Supplemental references

29. Marchiando AM, et al. A deficiency in the autophagy gene Atg16L1 enhances resistance to enteric bacterial infection. Cell Host Microbe. 2013; 14:216–24. [PubMed: 23954160]
30. Strong DW, Thackray LB, Smith TJ, Virgin HW. Protruding domain of capsid protein is necessary and sufficient to determine murine norovirus replication and pathogenesis in vivo. J Virol. 86:2950–8. [PubMed: 22258242]
31. Gonzalez-Hernandez MB, Bragazzi Cunha J, Wobus CE. Plaque assay for murine norovirus. J Vis Exp. :e4297.
32. Cadwell K, et al. A key role for autophagy and the autophagy gene Atg16l1 in mouse and human intestinal Paneth cells. Nature. 2008; 456:259–63. [PubMed: 18849966]
33. Robinson MD, McCarthy DJ, Smyth GK. edgeR: a Bioconductor package for differential expression analysis of digital gene expression data. Bioinformatics. 26:139–40. [PubMed: 19910308]
34. Huang da W, Sherman BT, Lempicki RA. Systematic and integrative analysis of large gene lists using DAVID bioinformatics resources. Nat Protoc. 2009; 4:44–57. [PubMed: 19131956]
35. Tajima M, Kotani Y, Kurosawa T, Miyasaka M. Pitfalls in mouse norovirus (MNV) detection in fecal samples using RT-PCR, and construction of new MNV-specific primers. Exp Anim. 62:127–35. [PubMed: 23615307]
36. Kim M, Lee H, Chang KO, Ko G. Molecular characterization of murine norovirus isolates from South Korea. Virus Res. 147:1–6. [PubMed: 19799947]
37. Izcue A, et al. Interleukin-23 restrains regulatory T cell activity to drive T cell-dependent colitis. Immunity. 2008; 28:559–70. [PubMed: 18400195]
38. Mumphrey SM, et al. Murine norovirus 1 infection is associated with histopathological changes in immunocompetent hosts, but clinical disease is prevented by STAT1-dependent interferon responses. J Virol. 2007; 81:3251–63. [PubMed: 17229692]

Europe PMC Funders Author Manuscripts

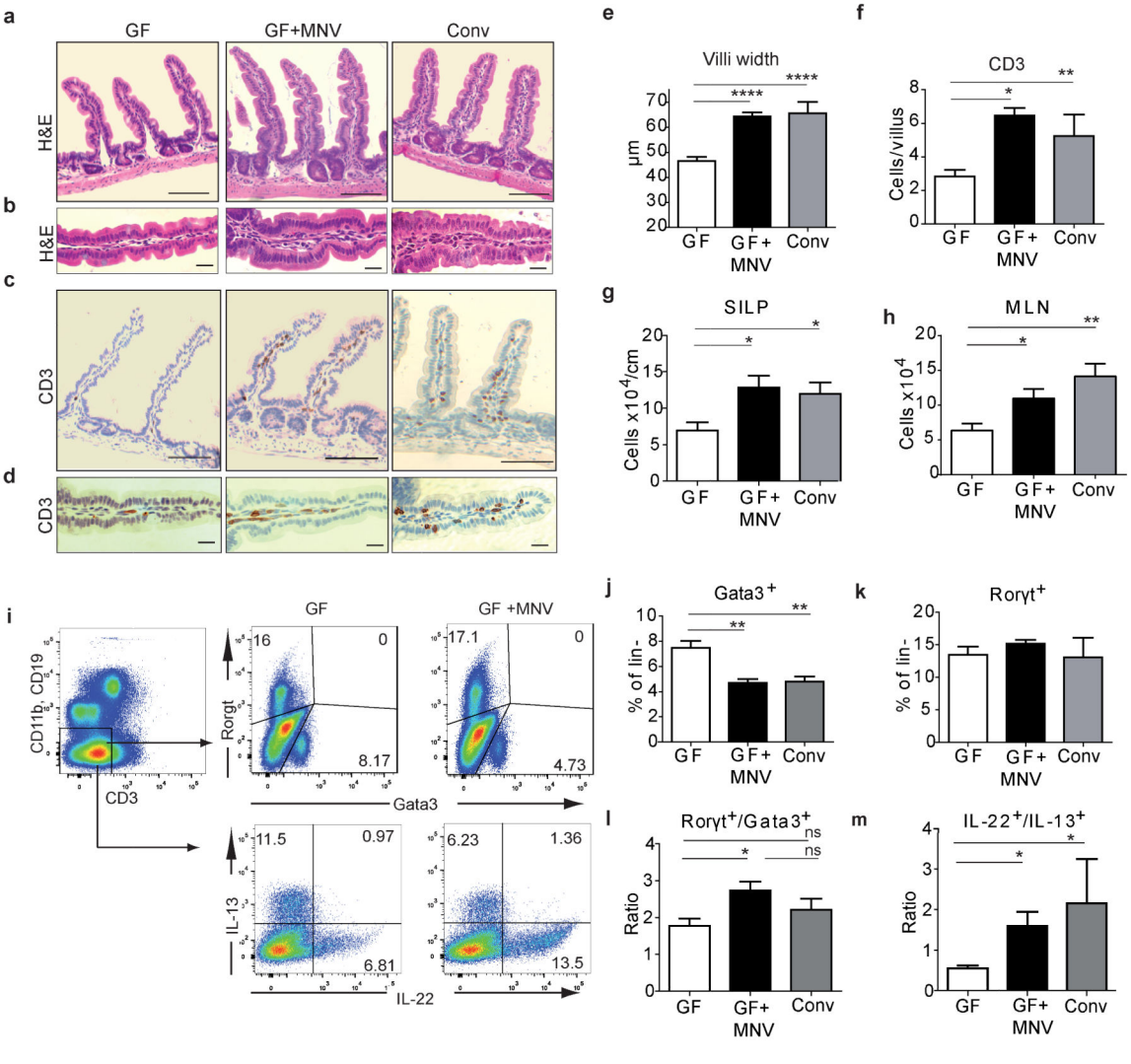

n

	GF	GF +MNV	Conv
villi width	-	++	++
Paneth cell granules and lysozyme expression	-	+	++
T cell numbers in LP and MLN	-	++	++
IFN-γ expression by T cells	-	+	++
antibody levels	-	++	++
intestinal ILC2	++	-	-

(-) minimum
(+) intermediate
(++) maximum
} value observed among the three conditions

Figure 1. MNV reverses intestinal abnormalities in germfree mice

(a,b) Representative small intestinal (SI) sections from germfree (GF), GF mono-associated with MNV.CR6 (GF+MNV), or conventional (Conv) mice stained with H&E (a,b) or anti-CD3 antibody (c,d). Scale bar = 100 μm in (a,d) and 10 μm in (c,d). **(e,f)** Quantification of villi width (e) and $CD3^+$ cells (f) per villus. 50 villi were quantified from 6-8 mice/group. **(g,h)** Total number of cells in the SI lamina propria (LP) and mesenteric lymph nodes (MLNs). N = 7-11 mice/group. **(i)** Flow cytometry analysis of SI LP cells for Gata3, Rorγt, IL-22, and IL-13 expression in live, lin^- cells ($CD11b^-$, $CD19^-$ and $CD3^-$). **(j-m)** Percent

Gata3^{+} (j) and Rorγt^{+} (k), and ratio of Rorγt^{+} to Gata3^{+} (l) and IL-22^{+} to IL-13^{+} (m) lin^{-} cells from (i). N = 10 mice/group. **(n)** Summary of comparisons between GF, GF+MNV, and Conv mice. GF+MNV have similar villi width, T cell numbers in SI LP and MLNs, and antibody levels as conventional mice and are designated (++) indicating restoration to the maximal value. GF+MNV display partial increases in the number of Paneth cell granules, lysozyme expression, and IFN-γ expression. For ILC2s, GF mice display the maximal value and GF+MNV are similar to Conv. ns: not significant, *p<0.05; **p<0.01; ****p<0.0001. Graphs display means ± SEM from at least two independent experiments.

Europe PMC Funders Author Manuscripts

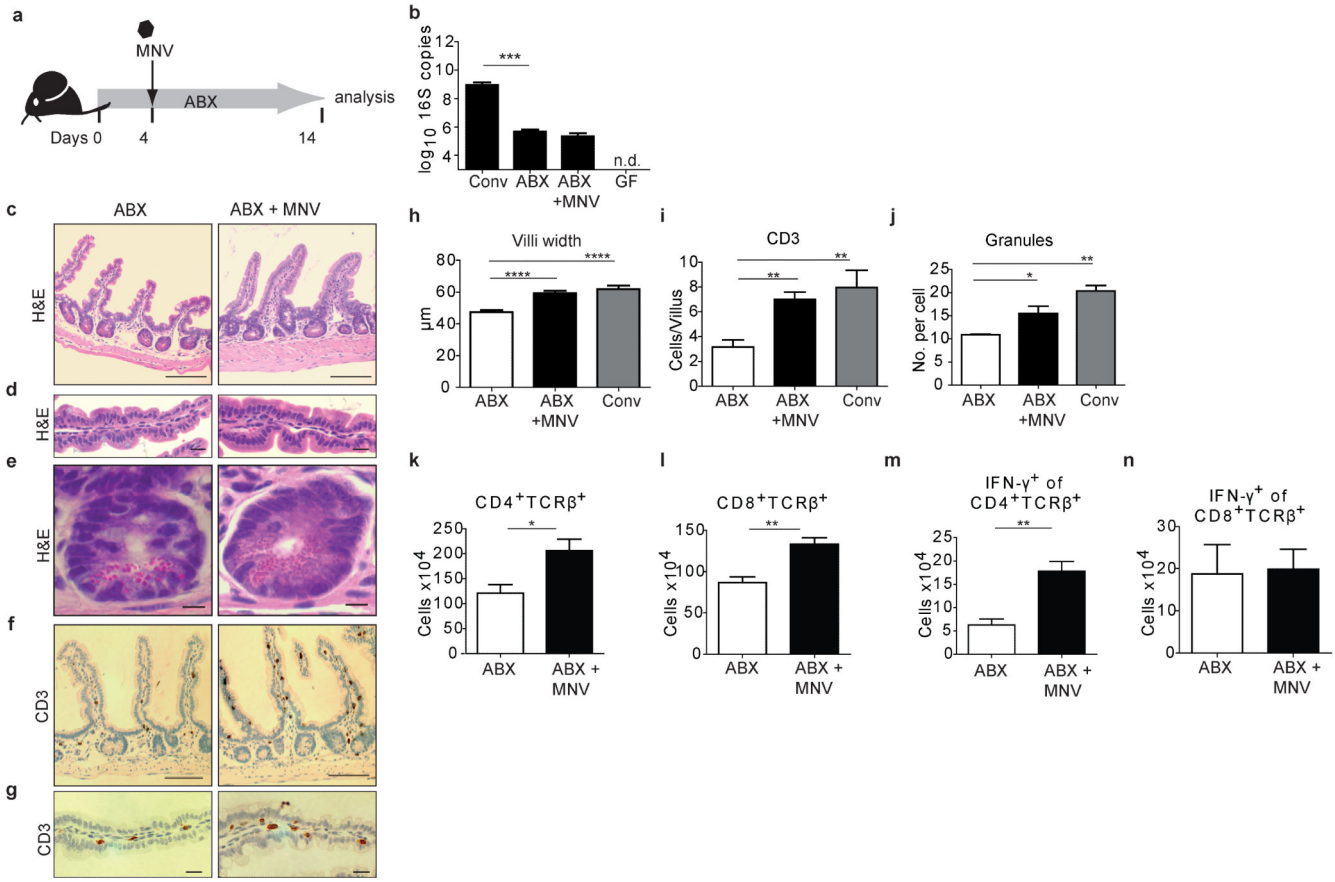

Figure 2. MNV reverses intestinal abnormalities induced by antibiotics

(a) Schematic for introducing MNV.CR6 into antibiotics (ABX)-treated mice (ABX+MNV). **(b)** 16S qRT-PCR analysis of stool from Conv, ABX-treated, ABX+MNV, and GF mice. n.d. = not detected. **(c-g)** Representative SI sections from ABX only and ABX+MNV mice stained with H&E or anti-CD3 antibody. Scale bars represent 100 μm in (c,f); 10 μm in (d,g) and 1 μm in (e). **(h-j)** Quantification of villi width (h), $CD3^+$ cells per villus (i), and granules per Paneth cell (j) for the mice in (c-g). N = 6-10 mice/group. **(k,l)** Number of $CD4^+$ (k) and $CD8^+$ T cells (l) in SI LP of ABX and ABX+MNV mice. **(m,n)** Number of IFN-γ^+ $CD4^+$ (m) and $CD8^+$ (n) T cells for mice in (k) and (l). *p<0.05; **p<0.01; ***p<0.001. Graphs display means ± SEM from at least two independent experiments

Europe PMC Funders Author Manuscripts

Europe PMC Funders Author Manuscripts

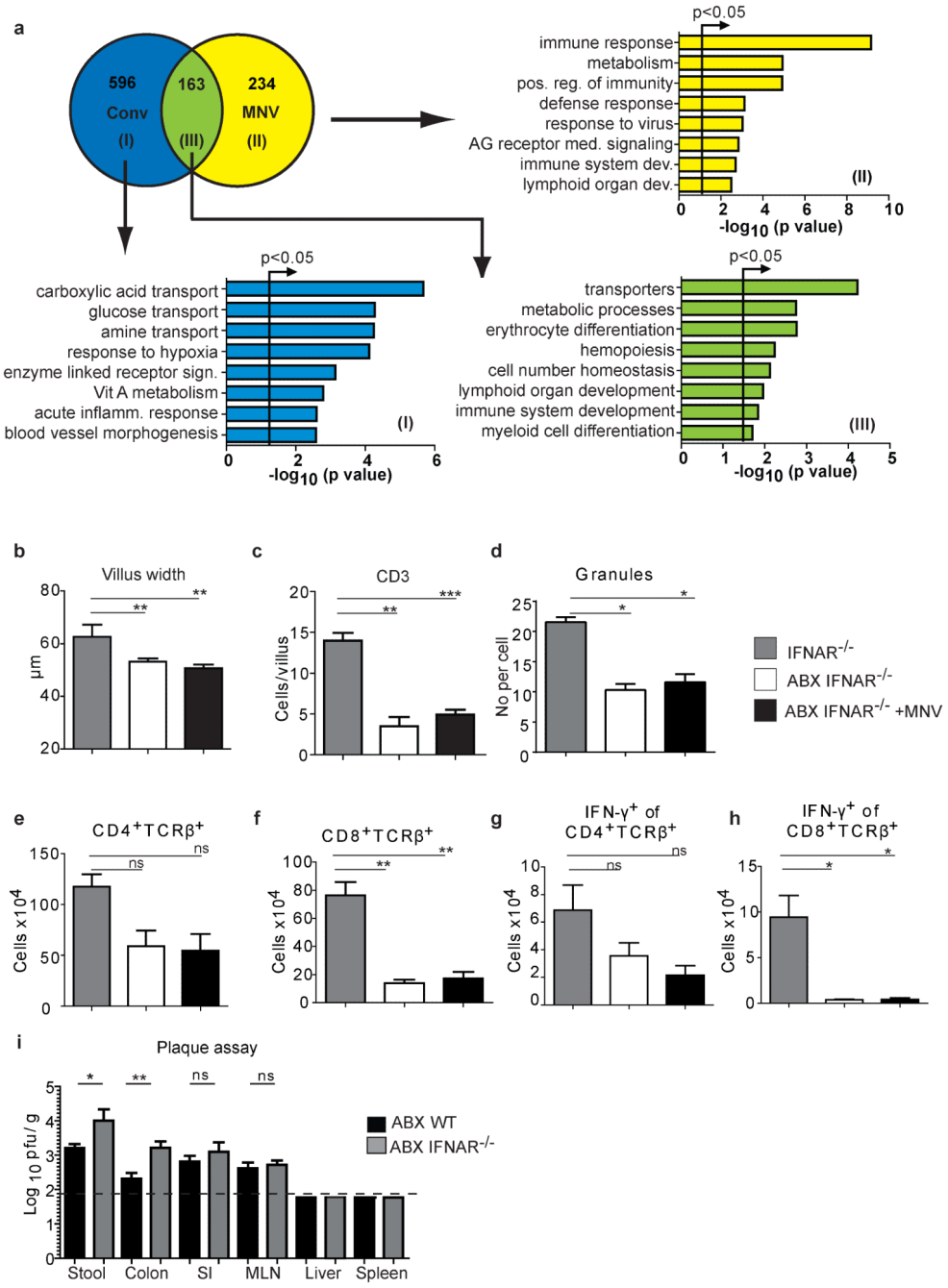

Figure 3. MNV induced changes are dependent on a type I interferon response

(a) RNA-seq analysis of SI tissue from GF mice inoculated with MNV.CR6, conventionalized with bacteria (Conv), or left untreated. Venn diagram represents number of transcripts displaying >1.4 fold enrichment upon conventionalization (I), inoculation with MNV.CR6 (II), or in both conditions (III) compared to untreated mice. Bar graphs represent gene ontology (GO) terms displaying association with the above gene sets. N = 3-4 mice. **(b-d)** Quantification of villus width (b), $CD3^+$ cells per villus (c) and granules per Paneth cells (d) of $IFNAR^{-/-}$ mice that received ABX, ABX+MNV.CR6, or left untreated. 50 villi or 30

crypts per mouse were quantified. N = 6 mice/group. **(e-h)** Total number of $CD4^+$ (e) and $CD8^+$ (f) T cells, and IFN-γ^+ $CD4^+$ (g) and $CD8^+$ (h) T cells in the SI LP of $IFNAR^{-/-}$ mice that received ABX, ABX+MNV.CR6, or left untreated. **(i)** Plaque forming units (pfu) of MNV.CR6 per cm tissue or per g stool from ABX-treated wild-type (WT) and $IFNAR^{-/-}$ mice 10 days post-infection. Dashed line denotes limit of detection. N = 3 mice/group. ns: not significant, *p<0.05; **p<0.01; ***p<0.001. Graphs display means ± SEM.

Europe PMC Funders Author Manuscripts

Europe PMC Funders Author Manuscripts

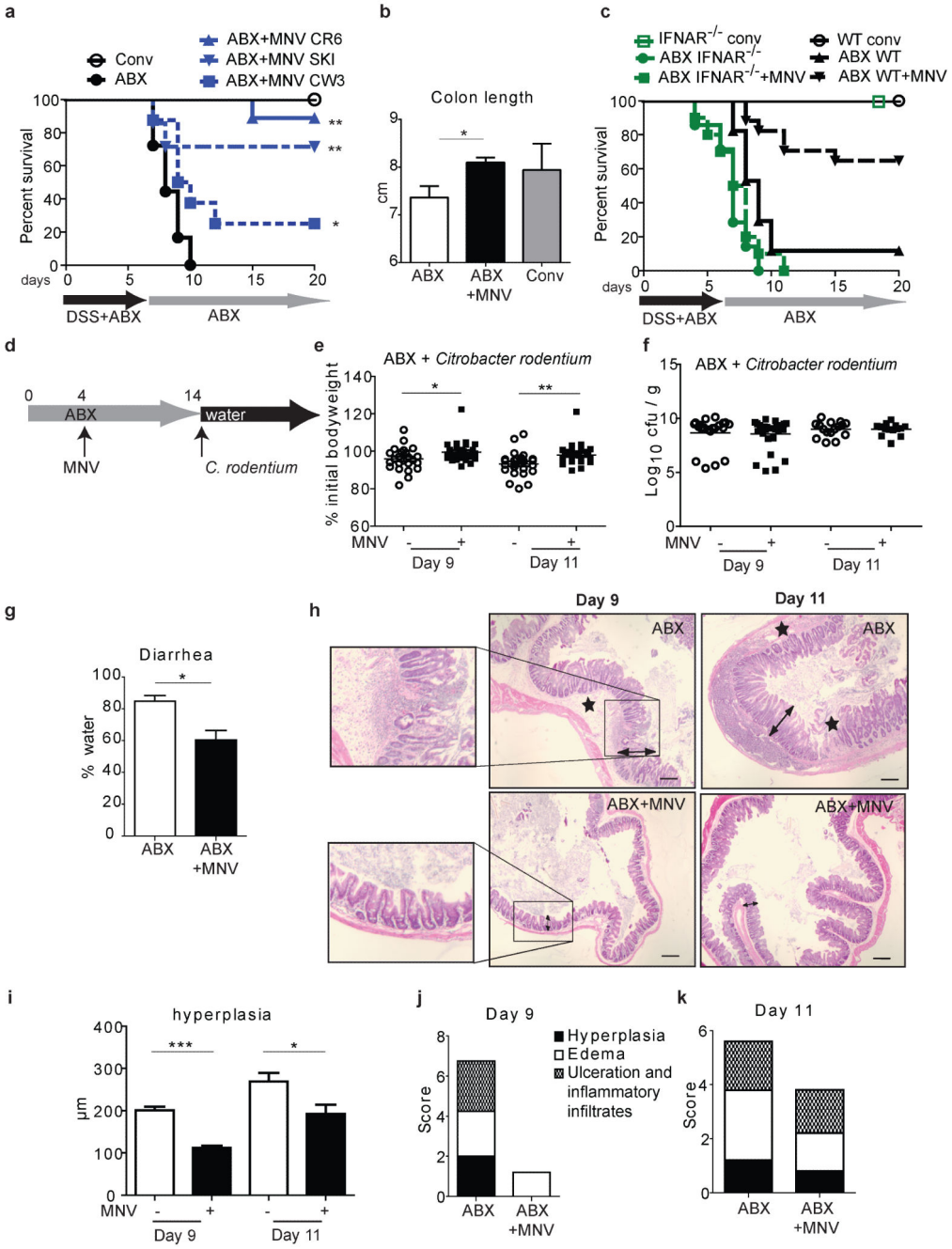

Figure 4. MNV protects antibiotics-treated mice from intestinal injury and *Citrobacter rodentium* super-infection

(a) Survival following DSS treatment of conventional mice (Conv), mice receiving ABX only, and mice receiving ABX and infected with indicated MNV strains. N = 12 mice/group. Statistical significance represents comparisons between ABX-treated mice infected with indicated MNV strains versus the ABX only group. **(b)** Colon length of Conv, ABX only, and ABX+MNV.CR6 mice on day 6 of DSS treatment. N = 3-5 mice/group. **(c)** Survival of conv WT and IFNAR$^{-/-}$, and ABX-treated WT and IFNAR$^{-/-}$ mice with and without

MNV.CR6 infection, treated with DSS. N = 7 mice/group. **(d)** Schematic of MNV.CR6 and *C. rodentium* co-infection in ABX-treated mice. ABX was removed prior to *C. rodentium* infection. **(e,f)** Quantification of weight loss (e) and colony forming units (cfu) in stool (f) in mice receiving treatment as illustrated in (d) on day 9 and 11 post-infection with *C. rodentium*. N = 5 mice/group. **(g)** Diarrhea from the above mice on day 9 post-infection. **(h-k)** Representative H&E-stained cecal sections (h) from above mice with arrows spanning hyperplasia and stars denoting ulceration and edema, quantification of hyperplasia (i), and histopathology score at day 9 and 11 (see methods) (j,k) (N = 5 mice/group). *p<0.05; **p<0.01; ***p<0.001. Bar graphs display means ± SEM and bars in (e) and (f) represent mean from at least two independent experiments.

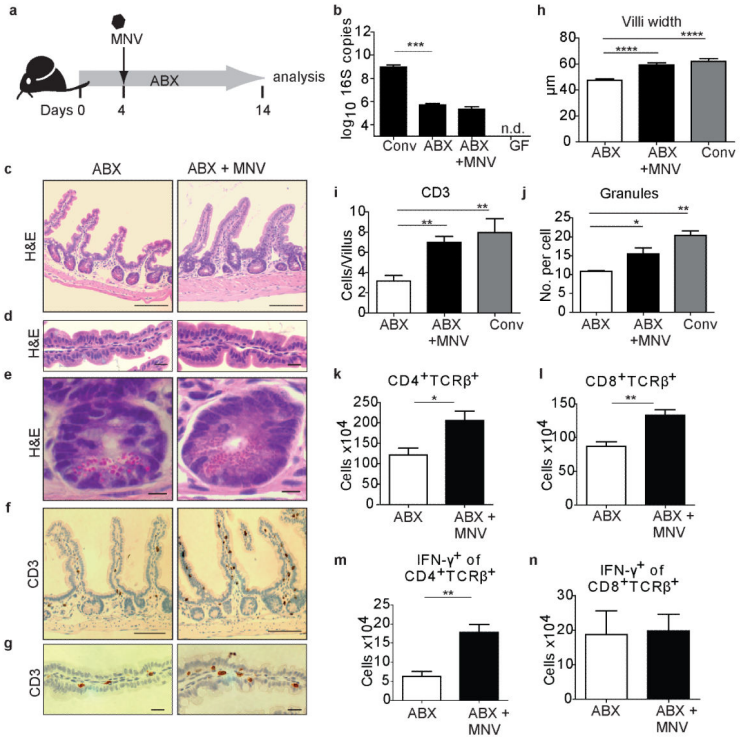

Figure 5.

Europe PMC Funders Author Manuscripts